Available online at www.sciencedirect.com
SCIENCE DIRECT®
ELSEVIER
Biochemical and Biophysical Research Communications 326 (2005) 147–153
BBRC
www.elsevier.com/locate/ybbrc

S100A4 inhibition by RNAi up-regulates osteoblast related genes in periodontal ligament cells

Chiyu Kato[a,b,*], Takehisa Kojima[a,b], Motohiro Komaki[a,b], Kaori Mimori[a,b], Wagner R. Duarte[c], Keizo Takenaga[d], Isao Ishikawa[a,b]

[a] *Periodontology, Department of Hard Tissue Engineering, Tokyo Medical and Dental University Graduate School, 1-5-45 Yushima, Bunkyo-ku, Tokyo 113-8549, Japan*
[b] *Center of Excellence Program for Frontier Research on Molecular Destruction and Reconstruction of Tooth and Bone, 1-5-45 Yushima, Bunkyo-ku, Tokyo 113-8549, Japan*
[c] *Dental Research Center, University of North Carolina at Chapel Hill, North Carolina 27599-7455, USA*
[d] *Division of Chemotherapy, Chiba Cancer Center Research Institute, 666-2 Nitona, Chuoh-ku, Chiba 260-8717, Japan*

Received 30 October 2004
Available online 19 November 2004

Abstract

Periodontal ligament (PDL) is a thin fibrous connective tissue located between alveolar bone and cementum that remains unmineralized physiologically. It is thus thought that PDL cells possess mechanisms to inhibit mineralization. It has been demonstrated that S100A4, a member of the S100 calcium-binding protein family, is synthesized and secreted by PDL cells, and that it may act as an inhibitor of mineralization. However, the mechanisms of action of S100A4 in mineralization have not been thoroughly clarified. In the present study we investigated the effects of S100A4 inhibition by a short interfering RNA (siRNA) on the expression of osteoblast related genes by human PDL cells. Inhibition of S100A4 by siRNA resulted in increased expression of osteoblastic markers such as osteopontin and osteocalcin, and the osteoblast-specific transcription factors, Runx2/Cbfa1 and Osterix. These results indicate that S100A4 suppresses the expression of osteoblastic genes in PDL cells and may thus inhibit mineralization in the PDL.

Keywords: Periodontal ligament; S100A4; siRNA; Runx2/Cbfa1; Osterix; Osteoblastic differentiation

Periodontal ligament (PDL) is a thin fibrous connective tissue situated between two mineralized tissues, i.e., alveolar bone and cementum. Despite the mechanical stress of mastication or orthodontic forces during orthodontic movement, under physiological conditions, the PDL maintains its width unmineralized. It has thus been speculated that PDL cells possess regulatory mechanisms to inhibit mineralization. Interestingly, under certain conditions, some cells within the PDL exhibit properties of osteoblasts and are capable of forming a mineralized matrix [1,2].

S100A4 is a member of the S100 calcium-binding protein family [3]. It has two calcium-binding motifs; one canonical EF-hand and another specific to the S100 family. Most of the proteins in this family are synthesized and localized intra-cellularly, and play fundamental roles such as cell metabolism, motility, and intra-cellular signaling [4,5]. S100A4 is known to be involved in motility and metastasis of cancer cells by interacting with cytoskeletal components. It is, therefore, considered a prognostic marker for cancer progression [6–8]. It is also reported that S100A4 is expressed in normal tissues such as smooth muscle, liver, bone marrow, smooth muscle cell of arteries, kidney, and osteoblastic cell in humans [9,10]. However, physiological functions

* Corresponding author. Fax: +81 3 5803 0196.
E-mail address: chiyu.peri@tmd.ac.jp (C. Kato).

0006-291X/$ - see front matter © 2004 Elsevier Inc. All rights reserved.
doi:10.1016/j.bbrc.2004.11.010

of S100A4 in normal tissues have not been thoroughly clarified.

Previous studies have shown that S100A4 was expressed by periodontal tissues and localized intra- and extra-cellularly in the PDL. Strutz et al. [11] demonstrated high gene expression of S100A4 in the periodontal mesenchyme during early stages of tooth development by in situ hybridization. It has been previously reported that the expression level of the S100A4 mRNA in bovine PDL is remarkably high when compared to other oral tissues such as dental follicle, dental papilla, and gingiva [12]. Furthermore, S100A4 is secreted from cultured bovine PDL cells and the addition of a recombinant mouse S100A4 protein inhibits mineralized nodule formation in cultured rat osteogenic cells in a dose-dependent manner [13]. These results suggest that S100A4 is localized in the PDL and may act as a negative regulator of mineralization. Moreover, in osteoblastic cell clones synthesizing low levels of S100A4, the formation of mineralized nodules was accelerated/increased and the mRNA expression of osteoblastic phenotypic markers was enhanced [14].

RNA interference (RNAi) is the process of sequence-specific, post-transcriptional gene silencing in animals and plants, initiated by double-stranded RNA (dsRNA) that is homologous in sequence to the silenced gene [15]. While the mechanism of RNAi is not yet fully understood, recent genetic and biochemical studies have revealed that RNAi is a useful technique for inhibition of specific gene expression. Elbashir et al. [15] showed that synthetic 21- to 23-nucleotide short interfering RNA (siRNA) could induce efficient RNAi in mammalian cells. Thus, RNAi has emerged as a powerful tool for silencing of gene expression in animals and plants.

In the present study, we employed the siRNA technique to inhibit S100A4 and investigated if S100A4 inhibition affects the expression of osteoblast-specific transcriptional factors and related genes in human PDL cells.

Materials and methods

Cell culture. Human PDL (hPDL) cells were obtained from healthy human teeth indicated for extraction for orthodontic treatment according to the report described by Somerman et al. [16]. Periodontal tissue was removed from the middle third of the root using a sterile scalpel. The tissue was rinsed five times with growth media (α-modified minimal essential medium, α-MEM; Gibco) and transferred to culture dishes.

Cultures were maintained in α-MEM supplemented with 10% fetal bovine serum (FBS; Gibco), in an atmosphere of 5% CO_2 in a humidified incubator. The medium was changed twice weekly. The cells were subcultured before reaching confluency.

siRNA transfection. siRNA, a double-stranded RNA (21 base pairs), was designed according to the siRNA design program si-Search [17] and modified for human S100A4 gene sequence as follows:

5′-GGA CAG AUG AAG CUG CUU UTT-3′,
5′-AAA GCA GCU UCA UCU GUC CTT-3′.

A mismatch siRNA (non-sense siRNA) of 21 base pairs was used as a negative control. Transfection of siRNA and non-sense siRNA was performed by the Oligofectamine kit (Invitrogen) according to the manufacturer's instructions. Briefly, hPDL cells were plated at 30% confluency with α-MEM without antibiotics. Before transfection, culture medium was changed to Opti-MEM Reduced Serum Medium (Gibco), and then siRNA and non-sense siRNA were transfected into the cells at the concentrations of 50–200 nM. Oligofectamine reagent alone (0 nM) was applied to the cells as a negative control. After 4 h, the medium was replaced with medium containing serum for further 72 h.

Immunostaining. Immunostaining was performed by the HISTOFINE kit (Nichirei). Briefly, hPDL cells were washed with phosphate-buffered saline (PBS), fixed with 10% formalin in PBS for 15 min at room temperature, and washed again with PBS. The cells were then treated with acetone/ethanol (50:50, vol/vol) for 1 min to permeate the cell membrane. After washing with PBS, the cells were incubated with rabbit polyclonal anti-mouse S100A4 antibody [7] (1:5 dilution with 1% BSA in PBS) or pre-immune rabbit serum for 3 h at room temperature. After the incubation, the cells were washed with PBS and further incubated with polyclonal anti-mouse IgG labeled with peroxidase for 1 h at room temperature. After washing with PBS, peroxidase substrate (diaminobenzidine) was applied to the hPDL cells for 3 min to develop color. Nuclei of hPDL cells were counterstained with hematoxylin. The cells were soaked in Carazzi's Hematoxylin solution for 30 min and washed with water three times. The staining was then observed under a light microscope. Total cells and positive stained cells were counted at randomly selected four fields per well and the average was used as the number of cells.

Reverse transcription-polymerase chain reaction analysis. Total RNA was extracted from cultured hPDL cells using the acid guanidinium thiocyanate–phenol–chloroform method. Cultured hPDL cells were washed two times with PBS and collected using sterile scrapers after the addition of RNAzol B (Cosmo Bio). RNA was recovered by phenol–chloroform extraction, precipitated with isopropanol, washed with 75% ethanol, and suspended in distilled water. UV absorbance at 260 and 280 nm was then measured and purity of RNA was confirmed by calculating the 260/280 ratio. Three micrograms of sample RNA was used for reverse transcription-polymerase chain reaction (RT-PCR) using SuperScript First-Strand Synthesis System for RT-PCR kit (Invitrogen) and AccuPrimer SuperMix I (Invitrogen). Primers specific for human S100A4, Runx2/Cbfa1, Osterix (Osx), osteopontin (OPN), osteocalcin (OCN), and GAPDH were designed as follows:

S100A4	5′-GGCCCTGGATGTGATGGTGT-3′
	5′-TCCACCACCCTGTTGCTGTA-3′
Runx2/Cbfa1	5′-GTGGACGAGGCAAGAGTTTCA-3′
	5′-TGGCAGGTAGGTGTGGTAGTG-3′
Osx	5′-CTTCAGTCTTCCCAACTTCTTACAC-3′
	5′-ACAAATTGGGTTAGCTACATCTCTG-3′
OPN	5′-TGACCTCTGTGAAAACAGCGT-3′
	5′-TGTACATTGTGAAGCTGTGAA-3′
OCN	5′-TTGTGTCCAAGCAGGAGGGCA-3′
	5′-ACATCCATAGGGCTGGGAGGT-3′
GAPDH	5′-ACCACAGTCCATGCCATCAC-3′
	5′-TCCACCACCCTGTTGCTGTA-3′

PCR was performed with annealing temperature of 60 °C (Runx2/Cbfa1), 51 °C (Osx), and 55 °C (others). After 30 (S100A4, GAPDH), 40 (Runx2/Cbfa1, Osx), and 45 (OPN, OCN) cycles, aliquots of the

PCR products were resolved on 1% TAE-agarose gels, stained with ethidium bromide, and photographed under ultraviolet light. To ensure that there are no artifacts in the RT-PCR procedure, we analyzed RT(−) sample as a negative control.

Quantitative real-time PCR. Quantitative real-time PCR was performed with the Light Cycler FastStart Master Sybr Green I (Roche Molecular Biochemicals) in a standard PCR using the Light Cycle-Primer Set Human GAPDH, and Human CBFA1 (Search GmbH). Each PCR was carried out in a total volume of 20 μl in glass capillaries containing 10 μl cDNA sample diluted with H_2O and 10 μl PCR mix. The cDNA sample was denatured at 95 °C for 10 min and added to the capillaries. The reaction was carried out using the following conditions for GAPDH and Runx2/Cbfa1: 35 cycles of 95 °C for 10 s, 68 °C for 10 s, and 72 °C for 16 s with a single fluorescence detection point at the end of the relevant annealing or extension segment. One cycle of melting curve from 58 to 95 °C by a transition rate of 0.1 °C/s with continuous detection of fluorescence was performed. The temperature transition rate for all amplifications was 20 °C/s. Analysis was carried out with the LightCycler Software Ver. 3.5 (Roche). The amount of the target gene was normalized to GAPDH. As a negative control, 10 μl of water without the cDNA template was also subjected to real-time PCR.

Statistical analysis. Unpaired Student's t test was used to detect statistical significance in the comparison of the percentage of S100A4 positive cells by immunostaining. Data are expressed as means ± standard deviation (SD).

Results

Expression of S100A4 after siRNA transfection in hPDL cells

mRNA expression of S100A4 in cultured hPDL cells 72 h after siRNA transfection was detected by semi-quantitative RT-PCR methods. Non-sense siRNA was also transfected as a control. The results of the semi-quantitative RT-PCR analysis of S100A4 are shown in Fig. 1. S100A4 mRNA was expressed in cultured hPDL cells. The expression was down-regulated after siRNA transfection, while no change was observed after non-sense siRNA transfection.

Immunostaining of S100A4 in cultured hPDL cells with or without siRNA transfection is shown in Fig. 2A. All the staining procedures were performed 72 h after the transfection. None of the cells were stained in the control experiments using pre-immune serum (Fig. 2A-a). Many hPDL cells were positively stained for S100A4 in the culture without siRNA transfection (Fig. 2A-b). The positive cells showed flatter and larger appearance that clearly distinguished from the negative cells. It is evident that the staining of S100A4 protein localized only in the cytoplasm as shown in higher magnification (Fig. 2B). The cultures with siRNA transfection showed fewer positive cells and the intensity of the staining decreased dose-dependently up to 100 nM (Fig. 2A-c, d). Fig. 2C shows the percentage of positive cells in cultures with different concentrations of siRNA. The percentage in the cultures with siRNA transfection decreased to 20–30% of that in the culture without transfection, indicating that siRNA transfection reasonably reduced S100A4 production.

mRNA expression of osteoblast phenotypic markers

mRNA expression of osteoblast phenotypic markers in cultured hPDL cells after siRNA transfection was detected by semi-quantitative RT-PCR and quantitative real-time PCR methods. The results of the semi-quantitative RT-PCR analysis of osteoblast phenotypic markers are shown in Fig. 3. S100A4 mRNA was constitutively expressed in control culture (0 nM). The expression of S100A4 was significantly down-regulated, when the cells were transfected with siRNA. In contrast, the expression of Osx, OPN, and OCN was clearly up-regulated. RT-PCR analysis for Runx2/Cbfa1 exhibited three bands. Intensity of the upper band was most intensive and appeared not to be varied by the siRNA transfection. Lower two bands (middle and lower bands) showed relatively lower intensity compared to that of the upper band, but the intensity appeared to be gradually increased by

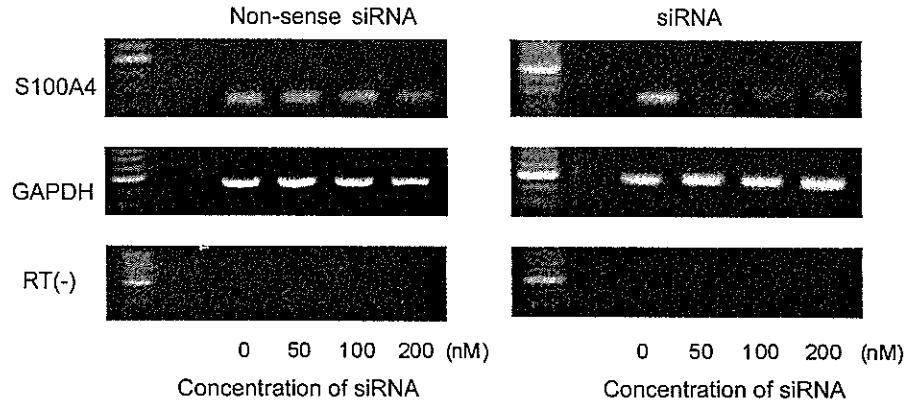

Fig. 1. mRNA expression of S100A4 72 h after siRNA or non-sense siRNA transfection. siRNA or non-sense siRNA was transfected into the cells at the concentrations of 50–200 nM. Oligofectamine reagent without siRNA (0 nM) was applied to the cells as a control. The expression of S100A4 mRNA in the human PDL cells was detected using semi-quantitative RT-PCR. The expression of S100A4 was down-regulated after siRNA transfection, whereas no change was observed after non-sense siRNA transfection. RT(−) sample was analyzed as a negative control.

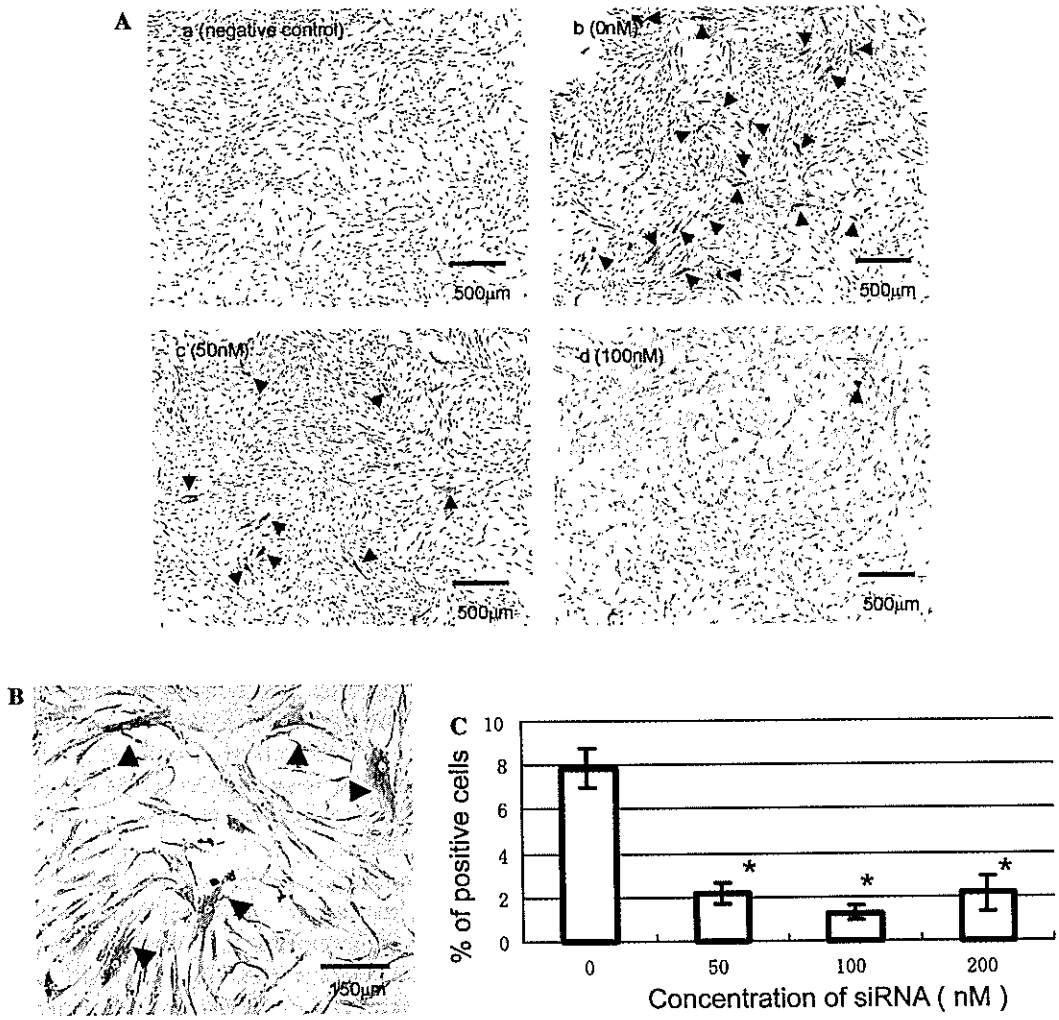

Fig. 2. (A) Immunostaining of S100A4 in cultured human PDL cells after siRNA transfection. All the staining procedures were performed 72 h after siRNA transfection. No staining was observed in the cells treated with pre-immune rabbit serum (a). In the culture without siRNA (b), many cells were positively stained. The positive cells (arrowheads) appeared flatter and larger comparing with negative cells. siRNA transfected cultures showed fewer positive cells (c,d). The intensity of the staining decreased dose-dependently up to 100 nM. Bars = 500 μm. Magnification 40×. (B) Cellular localization of S100A4 in hPDL cells (arrowheads). The staining of S100A4 localized only in the cytoplasm and no nuclear localization was detected. Bars = 150 μm. Magnification 100×. (C) The percentage of positive cells in cultures with different concentrations of siRNA. In the culture with siRNA transfection, the percentage of positive cells was significantly less compared to the control. Values are means ± SD ($n = 4$). *Significantly different from control ($P < 0.001$).

siRNA transfection in a dose-dependent manner. To analyze the expression level of Runx2/Cbfa1 more quantitatively, we performed quantitative real-time PCR analysis. The results revealed that the mRNA level of Runx2/Cbfa1 increased approximately 100- and 2000-fold after 50 and 100 nM siRNA transfection, respectively, at day 3 (Fig. 4). The increased Runx2/Cbfa1 expression could explain the up-regulation of Osx, OPN, and OCN, genes downstream to Runx2/Cbfa1.

Discussion

PDL cells are known to be a heterogeneous cell population and are indispensable for the regeneration of periodontal tissues including the unmineralized PDL and two mineralized tissues, i.e., cementum and bone [18].

S100A4 was detected in cultured hPDL cells at the protein and mRNA levels. Duarte et al. [14] have suggested that a decrease in S100A4 expression may be associated with a terminal osteoblastic differentiation and/or the initiation of mineralized matrix formation. Other reports have shown that the expression of S100A4 is high in osteoblast progenitors and decreases to undetectable levels in mature osteoblasts and in osteocytes [11,19]. These data suggest that S100A4 may play an important role both in PDL cells and osteoblasts in terms of regulation of osteoblastic differentiation/matrix mineralization.

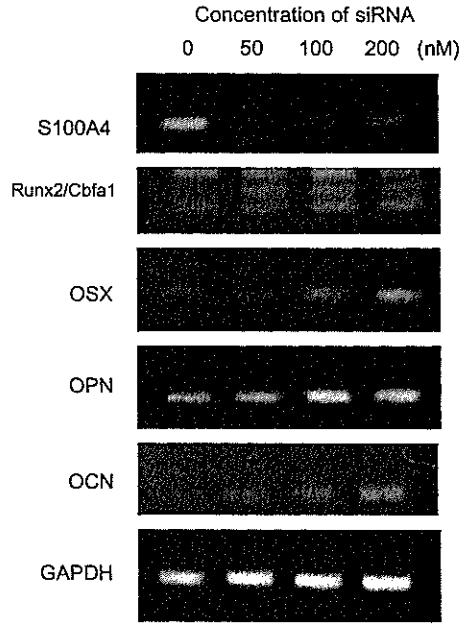

Fig. 3. mRNA expression of S100A4, Runx2/Cbfa1, Osterix (Osx), osteopontin (OPN), and osteocalcin (OCN) after siRNA transfection. siRNA was transfected into the cells at the concentrations of 50–200 nM. Oligofectamine reagent without siRNA (0 nM) was applied to the cells as a negative control. The expression levels of Runx2/Cbfa1, Osx, OPN, and OCN mRNA were up-regulated after siRNA transfection.

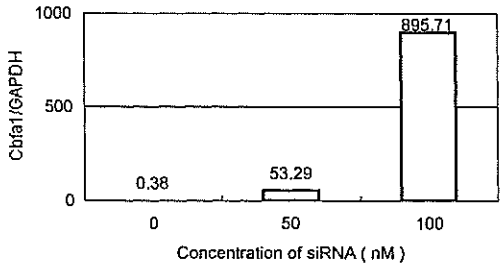

Fig. 4. Real-time PCR analysis of Runx2/Cbfa1 expression. *Y*-axis shows the ratio of Runx2/Cbfa1 to an internal control, GAPDH. mRNA level of Runx2/Cbfa1 increased approximately 100- and 2000-fold after 50 and 100 nM of siRNA transfection, respectively.

The application of RNAi has the potential to allow the systematic analysis of gene expression and holds the promise of therapeutic gene silencing [20–22]. A few limitations in the use of RNAi in mammalian cells have been reported [20,23], however, the recent development of 21-nucleotide siRNA duplexes has circumvented these problems and allowed successful RNAi in cultures of several types of mammalian cells [15,24]. Therefore, we used siRNA technique to inhibit S100A4 expression and investigate the potential physiological roles of S100A4 in human PDL.

Runx2/Cbfa1 and Osx are transcription factors required for osteoblastic differentiation. They are necessary for the commitment of osteoblasts, the expression of osteoblastic phenotypic genes, and bone formation [25–27]. The transfection of siRNA targeting S100A4 resulted in reduction of S100A4 expression and a dramatic increase in the expression level of Runx2/Cbfa1 at day 3 after the transfection. Saito et al. [28] reported that PDL cell line expressed Runx2/Cbfa1 at the same level to or even higher than that in osteoblasts in vivo, but the PDL cell line never mineralized, suggesting the presence of a mechanism responsible for suppressing the Runx2/Cbfa1 activity in PDL cells. Since the inhibition of S100A4 by siRNA enhanced Runx2/Cbfa1 expression in PDL cells, S100A4 could be one of the explanations for the suppressing mechanism. RT-PCR analysis for Runx2/Cbfa1 showed three different bands as reported previously for osteoblastic cell line and two isoforms (middle and lower bands in Fig. 3) appeared to be up-regulated by inhibition of S100A4. Although, Runx2/Cbfa1 has three different isoforms, i.e., cbfa1-3, the function of each isoform was not well understood [29]. Further experiments to figure out the function of Runx2/Cbfa1 isoforms are needed. Osx was also up-regulated after the transfection with the siRNA. Conversely, Duarte et al. [14] reported that the inhibition of S100A4 by antisense did not affect the mRNA level of Runx2/Cbfa1 or Osx expression after 5 and 10 days of induction of osteoblastic differentiation in a mouse osteoblastic cell culture. We assume that this difference may be in part due to a different experimental design, different time points to investigate Runx2/Cbfa1 expression, period of time the cells remained in culture prior to induction of differentiation, and possibly inter-species differences. Lee et al. [30] have reported that a transient up-regulation of transcription factors such as Runx2/Cbfa1 was observed during initial stages of osteoblastic differentiation. Therefore, we focused on relatively early time points such as day 3 after the siRNA transfection. It has been reported that Runx2/Cbfa1 expression is differentially regulated in human and rodent cells [31]. The immunostaining of hPDL cells showed that S100A4 expression was detected only in cytoplasm. On the other hand, recent report demonstrates that S100A4 localizes in the nucleus [32]. Although it is not clear whether S100A4 directly or indirectly regulates Runx2/Cbfa1 gene expression in hPDL cells, it is possible that inter-species difference is a key determinant in such regulation. Further study is required to clarify the mechanism of the regulation.

Inhibition of S100A4 in hPDL cells by the siRNA transfection also resulted in up-regulation of OPN and OCN, markers of osteoblastic differentiation. This result is in agreement with previous findings [14]. PDL cells are known to be heterogeneous containing osteogenic as well as non-osteogenic cells at various levels of differentiation [2,33–35]. Therefore, certain cells within the PDL may have the potential to form mineralized tissues such as cementum and alveolar bone [18], and it is likely that there are factors regulating mineralization at

physiological conditions. Our results indicate that S100A4 may be one of these factors playing a role as a negative regulator of mineralization by modulating the commitment of some PDL cells to osteoblastic differentiation. The present study provides only a short-term evaluation of these phenomena, since the optimal inhibitory effect of siRNA is reported to last 72 h after transfection and approximately 21 days of the culture required to detect mineralization in cultures of PDL cells [36,37]. Thus, long-term evaluation may be required to clarify the precise function of S100A4 in mineralization.

We conclude that S100A4 inhibition using siRNA resulted in up-regulation of osteoblastic differentiation markers in hPDL cells in culture. S100A4 may play an important role in regulation of mineralization in the PDL by modulating the commitment of some PDL cells to osteoblastic differentiation. To our knowledge, this is the first report to show the involvement of S100A4 in the regulation of osteoblast-specific transcription factors, Runx2/Cbfa1 and Osx.

Acknowledgments

This study was supported by Japan Society for the Promotion of Science (JSPS-B-4656) and Grant-in-Aid for Scientific Research of the Ministry of Education, Science, Sports and Culture of Japan (13470459).

References

[1] P. Lekic, C.A.G. McCulloch, Periodontal ligament cell populations: the central role of fibroblasts in creating a unique tissue, Anat. Rec. 245 (1996) 327–341.
[2] Y. Murakami, T. Kojima, T. Nagasawa, H. Kobaysashi, I. Ishikawa, Novel isolation of alkaline phosphatase-positive subpopulation from periodontal ligament fibroblasts, J. Periodontol. 74 (2003) 780–786.
[3] B.W. Schafer, R. Wicki, D. Engelkamp, M.G. Mattei, C.W. Heizmann, Isolation of a Yac clone covering a cluster of nine S100 genes on human chromosome 1q21: rationale for a new nomenclature of the S100 calcium-binding protein family, Genomics 25 (1995) 638–643.
[4] R. Donato, Functional roles of S100 proteins, calcium-binding proteins of the EF-hand type, Biochim. Biophys. Acta 1450 (1999) 191–231.
[5] B.W. Schafer, C.W. Heizmann, The S100 family of EF-hand calcium-binding proteins: functions and pathology, Trends Biochem. Sci. 21 (1996) 134–140.
[6] K. Takenaga, Y. Nakamura, H. Endo, S. Sakiyama, Involvement of S100-related calcium-binding protein pEL98 (or *mts 1*) in cell motility and tumor cell invasion, Jpn. J. Cancer Res. 85 (1994) 831–839.
[7] K. Takenaga, Y. Nakamura, S. Sakiyama, Y. Hasegawa, K. Sato, H. Endo, Binding of pEL98 protein, an S100-related calcium-binding protein, to nonmuscle tropomyosin, J. Cell Biol. 124 (1994) 757–768.
[8] G.V. Sherbet, M.S. Lakshmi, S100A4 (mts1) calcium-binding protein in cancer growth, invasion and metastasis, Anticancer Res. 18 (1998) 2415–2421.
[9] F.E.M. Gibbs, R. Barraclough, A. Platt-Higgins, P.S. Rudland, M.C. Wilkinson, E.W. Parry, Immunocytochemical distribution of the calcium-binding protein p9Ka in normal rat tissue: variation in the cellular location in different tissue, J. Histochem. Cytochem. 43 (1995) 169–180.
[10] K. Takenaga, Y. Nakamura, S. Sakiyama, Cellular localization of pEL98 protein, an S100-related calcium-binding protein, in fibroblasts and its tissue distribution analyzed by monoclonal antibodies, Cell Struct. Funct. 19 (1994) 133–141.
[11] F. Strutz, H. Okada, C.W. Lo, T. Danoff, R.L. Carone, J.E. Tomaszewski, E.G. Neilson, Identification and characterization of a fibroblast marker: FSP1, J. Cell Biol. 130 (1995) 393–405.
[12] W.R. Duarte, S. Kasugai, T. Iimura, S. Oida, K. Takenaga, K. Ohya, I. Ishikawa, cDNA cloning of S100 calcium-binding proteins from bovine periodontal ligament and their expression in oral tissues, J. Dent. Res. 77 (1998) 1694–1699.
[13] W.R. Duarte, T. Iimura, K. Takenaga, K. Ohya, I. Ishikawa, S. Kasugai, Extracellular role of S100A4 calcium-binding protein in the periodontal ligament, Biochem. Biophys. Res. Commun. 255 (1999) 416–420.
[14] W.R. Duarte, T. Shibata, K. Takenaga, E. Takahashi, K. Kubota, K. Ohya, I. Ishikawa, M. Yamauchi, S. Kasugai, S100A4: a novel negative regulator of mineralization and osteoblast differentiation, J. Bone Miner. Res. 18 (2003) 493–501.
[15] S.M. Elbashir, J. Harborth, W. Lendeckel, A. Yalcin, K. Weber, T. Tuschl, Duplexes of 21-nucleotide RNAs mediate RNA interference in cultured mammalian cells, Nature 411 (2001) 494–498.
[16] M.J. Somerman, R.A. Foster, G.M. Imm, J.J. Sauk, S.Y. Archer, Periodontal ligament cells and gingival fibroblasts respond differently to attachment factors in vitro, J. Periodontol. 60 (1989) 73–77.
[17] A.M. Chalk, C. Wahlestedt, E.L.L. Sonnhammer, Improved and automated prediction of effective siRNA, Biochem. Biophys. Res. Commun. 319 (2004) 264–274.
[18] S. Nyman, J. Gottlow, T. Karring, J. Lindhe, The regenerative potential of the periodontal ligament, J. Clin. Periodontol. 9 (1982) 257–265.
[19] J. Klingelhofer, N.S. Ambartsumian, E.M. Lukanidin, Expression of the metastasis-associated *mts 1* gene during mouse development, Dev. Dyn. 210 (1997) 87–95.
[20] P.D. Zamore, RNA interference: listening to the sound of silence, Nat. Struct. Biol. 8 (2001) 746–750.
[21] V. Mittal, Improving the efficiency of RNA interference in mammals, Nat. Rev. Genet. 5 (2004) 355–365.
[22] J.R. Bertrand, M. Pottier, A. Vekris, P. Opolon, A. Maksimenko, C. Malvy, Comparison of antisense oligonucleotides and siRNAs in cell culture and in vivo, Biochem. Biophys. Res. Commun. 296 (2002) 1000–1004.
[23] G.R. Stark, I.M. Kerr, B.R. Williams, R.H. Silverman, R.D. Schreiber, How cells respond to interferons, Annu. Rev. Biochem. 67 (1998) 227–264.
[24] S.S. Lakka, C.S. Gondi, N. Yanamandra, W.C. Olivero, D.H. Dinh, M. Gujrati, J.S. Rao, Inhibition of cathepsin B and MMP-9 gene expression in glioblastoma cell line via RNA interference reduces tumor cell invasion, tumor growth and angiogenesis, Oncogene (2004) 1–9.
[25] P. Ducy, R. Zhang, V. Geoffroy, A.L. Ridall, G. Karsenty, Osf2/Cbfa1: a transcriptional activator of osteoblast differentiation, Cell 89 (1997) 747–754.
[26] T. Komori, H. Yagi, S. Nomura, A. Yamaguchi, K. Sasaki, K. Deguchi, Y. Shimizu, R.T. Bronson, Y.H. Gao, M. Inada, M. Sato, R. Okamoto, Y. Kitamura, S. Yoshiki, T. Kishimoto, Targeted disruption of Cbfa1 results in a complete lack of bone formation owing to maturational arrest of osteoblasts, Cell 89 (1997) 755–764.

[27] K. Nakashima, X. Zhou, G. Kunkel, Z. Zhang, J.M. Deng, R.R. Behringer, B. Crombrugghe, The novel zinc finger-containing transcription factor osterix is required for osteoblast differentiation and bone formation, Cell 108 (2002) 17–29.
[28] Y. Saito, T. Yoshizawa, F. Takizawa, M. Ikegame, O. Iahibashi, K. Okubo, K. Hara, K. Ishibashi, M. Obinata, H. Kawashima, A cell line with characteristics of the periodontal ligament fibroblasts is negatively regulated for mineralization and Runx2/Cbfa1/Osf2 activity, part of which can be overcome by bone morphogenetic protein-2, J. Cell Sci. 115 (2002) 4191–4200.
[29] H. Harada, S. Tagashira, M. Fujiwara, S. Ogawa, T. Katsumata, A. Yamaguchi, T. Komori, M. Nakatsuka, Cbfa1 isoforms exert functional differences in osteoblast differentiation, J. Biol. Chem. 274 (1999) 6972–6978.
[30] M.H. Lee, A. Javed, H.J. Kim, H.I. Shin, S. Gutierrez, J.Y. Choi, V. Rosen, J.L. Stein, A.J. Wijnen, G.S. Stein, J.B. Lian, H.M. Ryoo, Transient upregulation of CBFA1 in response to bone morphogenetic protein-2 and transforming growth factor β1 in C2C12 myogenic cells coincides with suppression of the myogenic phenotype but is not sufficient for osteoblast differentiation, J. Cell. Biochem. 73 (1999) 114–125.
[31] C. Shui, T.C. Spelsberg, B.L. Riggs, S. Khosla, Changes in Runx2/Cbfa1 expression and activity during osteoblastic differentiation of human bone marrow stromal cells, J. Bone Miner. Res. 18 (2003) 213–221.
[32] K. Flatmark, K.B. Pedersen, J.M. Nesland, H. Rasmussen, G. Aamodt, S.O. Mikalsen, K. Bjomland, O. Fodstad, G.M. Malandsmo, Nuclear localization of the metastasis-related protein S100A4 correlates with tumor stage in colorectal cancer, J. Pathol. 200 (2003) 589–595.
[33] J.E. Piche, D.L. Carnes Jr., D.T. Graves, Initial characterization of cells derived from human periodontia, J. Dent. Res. 68 (1989) 761–767.
[34] R.M. Nohutcu, L.K. McCauley, Y. Shigeyama, M.J. Somerman, Expression of mineral associated proteins by periodontal ligament cells in vitro vs. ex vivo, J. Periodontal. Res. 31 (1996) 369–372.
[35] S. Ivanovski, H. Li, H.R. Haase, P.M. Bartold, Expression of bone associated macromolecules by gingival and periodontal ligament fibroblasts, J. Periodontal. Res. 36 (2001) 131–141.
[36] N. Arceo, J.J. Sauk, J. Moehring, R.A. Foster, M.J. Somerman, Human periodontal cells initiate mineral-like nodules in vitro, J. Periodontol. 62 (1991) 499–503.
[37] M.I. Cho, N. Matsuda, W.L. Lin, A. Moshier, P.R. Ramakrishnan, In vitro formation of mineralized nodules by periodontal ligament cells from the rat, Calcif. Tissue Int. 50 (1992) 459–467.

Hypoxia-Regulated Expression of Attenuated Diphtheria Toxin A Fused with Hypoxia-Inducible Factor-1α Oxygen-Dependent Degradation Domain Preferentially Induces Apoptosis of Hypoxic Cells in Solid Tumor

Nobuko Koshikawa[1,2] and Keizo Takenaga[1]

Divisions of [1]Chemotherapy and [2]Pathology, Chiba Cancer Center Research Institute, Chiba, Japan

Abstract

Tumor cells in hypoxic areas of solid tumors are resistant to conventional chemotherapy and radiotherapy and thus are obstacles of cancer therapy. We report here the feasibility of applying hypoxia-regulated expression of diphtheria toxin A (DT-A) for killing hypoxic tumor cells. The expression vector was constructed to express DT-A fused with hypoxia-inducible factor-1α (HIF-1α) oxygen-dependent degradation (ODD) domain under the control of vascular endothelial growth factor gene promoter and contain erythropoietin mRNA-binding protein (ERBP)–binding sequence downstream of the DT-A/ODD sequence. *In vitro* ubiquitination assay showed that DT-A/ODD, but not DT-A, was ubiquitinated as efficient as HIF-1α under normoxic conditions in a von Hippel-Lindau– and oxygen-dependent manner. DT-A/ODD exhibited a comparable translation inhibitory activity to DT-A. ERBP-binding sequence was effective in stabilizing mRNA under hypoxic conditions in various cell types. Transfection of the vector expressing DT-A/ODD into high-metastatic Lewis lung carcinoma (3LL) A11 cells resulted in induction of apoptosis independently of hypoxia, probably due to its extreme toxicity. However, transfection of the vector expressing attenuated DT-A^{W153F}/ODD or DT-A^{H21A}/ODD resulted in a hypoxia-dependent induction of apoptosis. Liposomal gene transfer of the vector encoding DT-A^{W153F}/ODD induced apoptosis in hypoxic, but not in normoxic, areas of solid tumors established by A11 variant cells with higher resistance to hypoxia-induced apoptosis and inhibited the growth of hypoxic tumors established by 3LL-P29 cells. These results suggest that hypoxia-regulated expression of attenuated DT-A^{W153F}/ODD fusion protein is potentially of use for killing hypoxic tumor cells with minimizing the damage to normoxic normal tissues. (Cancer Res 2005; 65(24): 11622-30)

Introduction

In most solid tumors, hypoxic areas are generated due to shortage of blood supply (1, 2). Because tumor cells in these hypoxic areas do not divide, they are resistant to conventional chemotherapy and radiotherapy (3). To make the matters worse, *in vivo* exposure of certain tumor cells to hypoxia followed by reoxygenation results in enhancement of invasive and metastatic potential (4). Recent studies have shown that tumor cells under hypoxic conditions overexpress Met and CRCX4 chemokine receptor and respond to hepatocyte growth factor and stromal cell–derived factor-1α, respectively, resulting in the stimulation of invasiveness and chemoattraction to organs that express stromal cell–derived factor-1α (5, 6). It has also been reported that $p53^{-/-}$ transformed cells and some of high-metastatic tumor cells are more resistant to hypoxia-induced apoptosis compared with $p53^{+/+}$ cells and low-metastatic cells, respectively (7, 8). Mutations, genetic instability, DNA overreplication, and gene amplification are frequently induced in hypoxic cells (9–11). These data collectively indicate that hypoxic tumor cells exhibit more aggressive phenotype than normoxic ones and potentially become more malignant, and thus eradication of hypoxic tumor cells is inevitable to cure cancer patients.

Tumor cells in hypoxic microenvironments produce vascular endothelial growth factor (VEGF) to stimulate neoangiogenesis (12). Hepatoma cells also produce erythropoietin (Epo) in response to hypoxia (13). Hypoxic induction of VEGF and Epo is regulated at both transcriptional and posttranscriptional levels (14). Hypoxia activates the transcriptional complex termed hypoxia-inducible factor-1 (HIF-1), which is a heterodimer composed of an oxygen-regulated α subunit (HIF-1α) and a constitutively expressed β-subunit (HIF-1β/aryl hydrocarbon receptor nuclear translocator), both subunits being members of a subfamily of basic helix-loop-helix proteins that contain a conserved PAS domain (15, 16). HIF-1 binds to the hypoxia response element located upstream of the *VEGF* gene or downstream of the *Epo* gene and transactivates its expression (17). In normoxic conditions, HIF-1α is hydroxylated at two proline residues in the oxygen-dependent degradation (ODD) domain by HIF prolyl hydroxylases, recognized by the von Hippel-Lindau (pVHL)/Elongin B/Elongin C/Cul2 E3 ligase complex, and then subjected to rapid ubiquitination followed by proteasomal degradation (18, 19). When exposed to hypoxia, the activity of HIF prolyl hydroxylases is down-regulated and subsequently HIF-1α is rapidly stabilized (20, 21). The posttranscriptional regulation of *VEGF* and *Epo* mRNA involves the stabilization of the mRNA by the RNA-binding protein HuR and *Epo* mRNA-binding protein (ERBP), respectively, the binding site of which resides in the mRNA 3′-untranslated region (UTR; refs. 22, 23).

Hypoxia can be regarded as a physiologic abnormality that is restricted to the tumor; thus, it can be used as a trigger for heterologous gene expression. In fact, others and we have shown that hypoxia response element–regulated expression of prodrug-activating enzymes can sensitize hypoxic tumor cells to the corresponding prodrugs (24–27). Principally, however, this strategy is probably ineffective to quiescent tumor cells under hypoxic circumstances. Moreover, poor perfusion may limit prodrug

Requests for reprints: Keizo Takenaga, Division of Chemotherapy, Chiba Cancer Center Research Institute, 666-2 Nitona, Chuoh-ku, 260-8717 Chiba, Japan. Phone: 81-43-264-5431; Fax: 81-43-265-4459; E-mail: keizo@chiba-cc.jp.

doi:10.1158/0008-5472.CAN-05-0111

diffusion to hypoxic regions. Therefore, to kill hypoxic tumor cells that are quiescent and insensitive to conventional chemotherapeutic agents, it is desirable to use a method that ensures cell death once a heterologous gene is expressed in the cells.

Diphtheria toxin A chain (DT-A) is the component of diphtheria toxin that inhibits protein synthesis in susceptible cells. It directly binds NAD^+ and catalyzes the transfer of ADP ribose from NAD^+ to elongation factor 2, which irreversibly inhibits elongation factor 2 (28). *DT-A* gene has been considered to be applicable for cancer gene therapy (29–34). Because DT-A leads to rapid cell cycle–independent death, it might be useful to kill hypoxic tumor cells if its expression is properly regulated. However, because of its extreme toxicity, it is hard to reduce nonspecific cytotoxicity (35). Nevertheless, several strategies that limit its toxicity have been developed and those include targeted delivery of DT-A to specific cells or tissue-specific expression, such as DT-A immunotoxin (30), DT-A fused to peptide ligands for cell-specific receptor (32), and DT-A expression construct under the control of a regulatory element or tissue-specific promoter (31, 33, 34). With regard to cancer gene therapy, α-fetoprotein promoter and prostate-specific antigen promoter–regulated expression of *DT-A* gene led to selective killing of hepatocarcinoma cell lines and prostate cancer cell lines, respectively, by using a liposomal gene transfer system (33, 34). In other cases, however, although preferential killing of target tumor cells could be shown, nonspecific cytotoxicity could not be abolished due to the background expression of DT-A (35).

In the present study, we examined the feasibility of application of *DT-A* gene for killing hypoxic tumor cells. To induce hypoxia-dependent expression of DT-A, we constructed an expression vector harboring wild-type or attenuated *DT-A* gene under the control of VEGF promoter. To increase hypoxia specificity, we designed the expression vector to express DT-A fused with HIF-1α ODD domain, expecting that the fusion protein is rapidly ubiquitinated and degraded through proteasome pathway in normoxia but stabilized in hypoxia. In addition, we constructed it to express mRNA containing ERBP-binding sequence (EBBS), aiming for stabilization of the mRNA in hypoxia. We report here that expression of attenuated DT-A^{W153F}/HIF-1α ODD fusion protein driven by VEGF promoter causes efficient cell death of hypoxic tumor cells *in vitro* and *in vivo*.

Materials and Methods

Cells and Cell Culture

Highly metastatic A11 cells and low-metastatic P29 cells are derived from Lewis lung carcinoma and their characteristics are described elsewhere (25). pVHL-deficient human renal carcinoma 786-O and their transfectants stably expressing wild-type pVHL (referred herein as 786-O/VHL cells) were generously provided by Dr. Y. Nagashima (Yokohama City University School of Medicine, Yokohama, Japan). Human hepatoma HepG2 cells were obtained from Human Science Research Resources Bank (Osaka, Japan). The cells were cultured at 37°C in DMEM supplemented with heat-inactivated 10% fetal bovine serum, 100 units/mL penicillin, and 100 μg/mL streptomycin. They were also cultured under hypoxic environment (1% O_2) generated in NAPCO automatic O_2/CO_2 incubator (Precision Scientific, Chicago, IL). A11H10 cells were established after exposing A11 cells 10 times to severe hypoxia (<0.1% O_2, generated in GasPak Pouch, Becton Dickinson, Cockeysville, MD) reoxygenation cycle.

Plasmid Constructions

pVEGFpro-DT-A/ODD-EBBS expression plasmid. To avoid the effect of enhancer/promoter sequence that an expression vector usually contains for driving a drug selection marker gene, we used the backbone of pGL3-basic (Promega, Madison, MD) to construct the DT-A/ODD expression vector. First, EBBS corresponding to 117 nucleotides downstream of the stop codon of *Epo* mRNA was prepared by reverse transcription-PCR (RT-PCR) using total RNA isolated from HepG2 cells and the sense primer 5′-CCAGGTGTGTCCACCTGGGC-3′ and the antisense primer 5′-GACAGG-CTGGCGCTGAGCTG-3′. The resulting PCR product was subcloned into pGEM-T Easy vector (Promega) and the insert was cut out with *Not*I, gel-purified, and then inserted into the *Not*I site of pcDNA3 to make a plasmid pcDNA3-ERBP. Next, the nucleotide sequence of ODD domain corresponding to the amino acid residues 396 to 618 of human HIF-1α was amplified by RT-PCR using total RNA isolated from HepG2 cells and the sense primer 5′-ACAGGGGACAGATGACCAGG-3′ and the antisense primer 5′-TCAGGCGTCTTCCCAGCATG-3′. After subcloning in pGEM-T Easy vector, the insert was cut out with *Sal*I and *Xho*I, gel-purified, and ligated to the *Sal*I/*Xho*I cut pIBI-DT-A plasmid (kindly provided by Dr. Gail Harrison, University of Colorado Health Sciences Center, Denver, CO). The intrinsic stop codon TAG of *DT-A* gene was then changed to TTG by using Mutan-Express Km kit (TaKaRa Biomedicals, Osaka, Japan) and the oligonucleotide 5′-GGTCGACTCAAGAGGATCCC-3′ so that DT-A fuses with ODD in frame. The resulting plasmid was digested with *Nru*I and *Aat*I, blunt-ended by T4 DNA polymerase, and ligated to the *Eco*RV-cut pcDNA3-EBBS to make a plasmid pcDNA3-DT-A/ODD-EBBS. The resulting plasmid was digested with *Nco*I and *Xba*I, and the DT-A/ODD-EBBS cassette was gel-purified, blunt-ended, and then ligated to the *Nco*I/*Xba*I cut, blunt-ended pGL3-basic to make a plasmid pGL3-DT-A/ODD-EBBS. The VEGF promoter sequence of the phVEGF-1 plasmid (kindly provided by Dr. H. Esumi, National Cancer Center Research Institute East, Tokyo, Japan; ref. 36) was digested with *Kpn*I and *Nhe*I, gel-purified, and ligated to the *Kpn*I/*Nhe*I-cut pGL3-basic or pGL3-DT-A/ODD-EBBS, yielding a plasmid pVEGFpro or pVEGFpro-DT-A/ODD-EBBS, respectively. The plasmid-harboring attenuated DT-A, pVEGFpro-DT-A^{W153F}/ODD-EBBS, was made by changing the codon TGG to TTT, resulting in the amino acid change from tryptophan 153 to phenylalanine by using Transformer Site-Directed Mutagenesis kit (BD Sciences Clontech, Tokyo, Japan). pVEGFpro-DT-A^{H21A}/ODD-EBBS was made in a similar way by changing the codon CAC to GCC, resulting in the amino acid change from histidine 21 to alanine. All of the nucleotide sequence prepared by RT-PCR and mutagenesis were confirmed by nucleotide sequencing.

Luciferase reporter plasmid harboring erythropoietin mRNA-binding protein-binding sequence. The EBBS in pGEM-T Easy prepared as above was digested with *Eco*RI, blunt-ended, and then ligated to the pflM1 cut, blunt-ended pGL2-basic (Promega). The VEGF promoter sequence was then inserted into the *Kpn*I/*Nhe*I site of the plasmid to make a plasmid pVEGFpro-Luc-EBBS.

In vitro Ubiquitination Assay

In vitro ubiquitination assay was done as described previously (37). Briefly, DT-A and HIF-1α radiolabeled with ^{35}SPRO-MIX (Amersham Biosciences Corp., Piscataway, NJ) were prepared by *in vitro* transcription and translation of genes subcloned into pcDNA3 using the TNT T7 Quick Coupled Transcription/Translation System (Promega). To prepare cell extracts (S100 fraction), 293T cells were washed twice with ice-cold hypotonic extraction buffer [20 mmol/L Tris-HCl (pH 7.5), 5 mmol/L KCl, 1.5 mmol/L $MgCl_2$, and 1 mmol/L DTT]. After removal of the buffer, cells were disrupted in a Dounce homogenizer. Following cell lysis, crude extract was centrifuged at 10,000 × *g* for 10 minutes at 4°C. The supernatant was collected and further centrifuged at 100,000 × *g* for 4 hours at 4°C. The resulting cell extract (S100 fraction) was stored in aliquot at −80°C. Ubiquitination assays were done at 30°C in a total volume of 20 μL composed of 2.5 μL of programmed reticulocyte lysate, 83 μg of S100 fraction, 2 μL of 10 × ATP-regenerating system [20 mmol/L Tris-HCl (pH 7.5), 10 mmol/L ATP, 10 mmol/L magnesium acetate, 300 mmol/L creatine phosphate, and 0.5 mg/mL creatine phosphokinase], 1 μL of 10 mg/mL ubiquitin (Sigma-Aldrich, St. Louis, MO), or 10 mg/mL ubiquitin aldehyde (Boston Biochem, Cambridge, MA). Aliquots were removed at indicated times, mixed with SDS sample buffer, and analyzed by 12.5% SDS-PAGE followed by autoradiography.

In vitro Assay of Translation Inhibitory Activity of Diphtheria Toxin A

Translation inhibitory activities of DT-A, DT-A/ODD, and its attenuated fusion proteins were assayed as described (38) with some modifications. First, DT-A proteins were prepared by *in vitro* transcription/translation of genes subcloned into pcDNA3 using TNT T7 Quick Coupled Transcription/Translation System. Then, 1 μL of the translated DT-A protein was added to 11 μL of TNT SP6 Quick Coupled Transcription/Translation mixture containing 0.5 μg of NAD^+, 0.45 μL ^{35}SPRO-MIX, and 250 ng of luciferase SP6 control DNA (Promega). The samples were incubated for 90 minutes at 30°C and the proteins were separated on 12.5% SDS-PAGE and detected by autoradiography.

Luciferase Reporter Assay

For examining the effect of EBBS, the luciferase reporter plasmid, pVEGFpro-Luc or pVEGFpro-Luc-EBBS, was transiently transfected into cells using Lipofectin (Invitrogen Corp., Carlsbad, CA). As a control for transfection efficiency, pRL-CMV vector (Promega) was cotransfected with test plasmids. pGL2-control vector (Promega) was used as a positive control. Luciferase activity in cell extracts was assayed 48 hours posttransfection according to Dual-Luciferase reporter assay system protocols (Promega) using a luminometer (model TD-20/20, Turner Designs, Sunnyvale, CA).

RNA Extraction and Northern Blot Analysis

Total RNA was extracted with guanidinium thiocyanate from cells cultured under normoxic or hypoxic environment. Total RNA (20 μg) was electrophoresed on 1% agarose gel containing formaldehyde and transferred to nylon filters. Blots were hybridized with a ^{32}P-labeled mouse *VEGF* cDNA probe, which was prepared by the random primer method. Filters were finally washed at 50°C in 30 mmol/L NaCl, 3 mmol/L sodium citrate, and 0.1% SDS.

Assays for Apoptosis

Chromatin condensation and fragmentation were visualized by staining the cells with 4′,6-diamidino-2-phenylindole (DAPI, 10 μg/mL; ref. 8). Annexin V staining was done using Annexin V–enhanced green fluorescent protein (EGFP) apoptosis detection kit (MBL, Nagoya, Japan), according to the instructions of the manufacturer. Fluorescence was observed under a Fluoview confocal laser microscope (Olympus, Tokyo, Japan). Flow cytometric analysis was done as described previously (8) to analyze cellular DNA fragmentation with a FACScan flow cytometer (Becton Dickinson, Mountain View, CA). Cell death was monitored by trypan blue dye exclusion.

In vivo Gene Transfer and Detection of Hypoxic Areas and Apoptosis in Tumors

A11H10 cells (5×10^5 cells) were inoculated s.c. into the abdominal flank of female C57BL/6 mice (Nippon SLC, Shizuoka, Japan). Twelve days after the inoculation, when an estimated tumor volume reached ~800 mm^3, DNA/liposome complex that is composed of 40 μg of pEGFP-N1, pVEGFpro or pVEGFpro-DT-A^{W153F}/ODD-ERBP, 40 μL of DMRIE-C (Life Technologies, Tokyo, Japan), and 5 μg of MW 70,000, lysine-fixable dextran-tetramethylrhodamine conjugates (dextran-TMR, Molecular Probes, Inc., Eugene, OR) in 200 μL Opti-MEM was directly injected intratumorally. Two days after the injection, 300 μL of EF5 solution (3 mg/mL) were administered i.p. into mice bearing s.c. tumors (39). One hour later, tumors were surgically removed and frozen in optimum cutting temperature compound. Cryostat sections cut at 10 μm were fixed with 4% paraformaldehyde and washed with Dulbecco's PBS (DPBS). To detect apoptotic tumor cells, terminal deoxynucleotidyl transferase–mediated dUTP nick-end labeling (TUNEL) stainings were done on the sections using ApopTag Fluorescein *In situ* Apoptosis Detection kit (Serologicals Corp., Norcross, GA), according to the instructions of the manufacturer. The sections were then treated with 5% mouse serum, 20% dry milk, and 0.3% Tween 20 in DPBS overnight at 4°C to block nonspecific binding sites. They were rinsed with 0.3% Tween 20 in DPBS and then incubated with Cy5-labeled monoclonal anti-EF5 antibody (ELK3-51) for 4 hours at 4°C to detect hypoxic regions in the tumors. After extensive washing with DPBS, tissue samples were counterstained with Hoechst 33324 and observed under a fluorescence microscope. Images were captured using a Cool SNAP charge-coupled device camera and processed by a RS IMAGE Express image processing software (Nippon Roper, Chiba, Japan).

In vivo Gene Transfer and Tumor Growth

P29 cells (4×10^5) were inoculated s.c. into the abdominal flank of female C57BL/6 mice (10 mice per group). Ten days after the inoculation, DNA/liposome complex (12 μg of pVEGFpro or pVEGFpro-DT-A^{W153F}/ODD-ERBP and 3 μL of DMRIE-C in 200 μL of Opti-MEM) was directly injected into the tumor. The injection was done daily until the end of the experiments. Tumor growth was monitored by caliper measurement of two diameters at right angles and the tumor mass was estimated from the equation, volume = $0.5 \times a \times b^2$, where a and b are the larger and smaller diameters, respectively.

Determination of the Degree of Hypoxia in Subcutaneous Tumors

A11H10 and P29 cells (1×10^6) were inoculated s.c. into C57BL/6 mice. When tumor volumes reached ~650 mm^3, the mice were injected with EF5. Cryostat sections of the tumors were made at every 400 μm distance and stained with Cy3-labeled monoclonal anti-EF5 antibody (ELK3-51) as described above. For analyzing EF5-positive (hypoxic) areas on each section, at least five randomly selected fluorescent images were captured with a Leica fluorescence microscope system equipped with a computer. The images were transferred to the ImageJ 1.34s software and EF5-positive areas were analyzed. In this way, >100 fields (1.175 mm^2/field) were analyzed and the percentage of EF5-positive area per field was calculated.

Results

Oxygen and von Hippel-Lindau–dependent ubiquitination of DT-A/ODD fusion protein. To examine the effect of HIF-1α ODD domain on ubiquitination of DT-A/ODD fusion protein, we subjected the *in vitro* translated ^{35}S-labeled DT-A/ODD proteins to the *in vitro* ubiquitination assay. Incubation of DT-A/ODD with cell extract from 293T cells alone resulted in the appearance of a slower migrating form (Fig. 1*A*). The effect was enhanced by the addition of ATP generation system. Addition of ubiquitin resulted in a further mobility shift of these species. These results indicated that these mobility shifts were most likely due to ubiquitination of DT-A/ODD proteins. This was confirmed by a further shift of these species to high molecular weight proteins by the addition of ubiquitin aldehyde, an isopeptidase inhibitor that prevents the degradation of ubiquitin conjugates. Ubiquitination of DT-A/ODD, but not of DT-A that served as a control, proceeded as the incubation time prolonged (Fig. 1*B*), which was comparable with that of HIF-1α proteins (Fig. 1*C*). Addition of desferrioxamine, a hypoxia mimetic, to the reaction mixture inhibited DT-A/ODD ubiquitination in a dose-dependent manner (Fig. 1*D*). Furthermore, ubiquitination of the protein was more prominent in 786-O/VHL cells than in 786-O cells, although a low level of DT-A/ODD ubiquitination was apparent in 786-O cells (Fig. 1*E*). Taken together, these results indicate that DT-A/ODD, but not DT-A, is ubiquitinated dependently on oxygen and pVHL.

Effect of erythropoietin mRNA–binding protein binding sequence on the expression level of luciferase under hypoxic conditions. To examine the effect of EBBS on the expression level of a heterologous gene, we constructed luciferase reporter plasmids, pVEGFpro-Luc as a control and pVEGFpro-Luc-EBBS (Fig. 2*A*). After transient transfection of each reporter plasmid into A11 or HepG2 cells, they were exposed to hypoxia for 18 hours and then luciferase activity was measured. As shown in Fig. 2*B* and *C*, although integration of EBBS into the reporter plasmid resulted in an increase in the luciferase activity under normoxic conditions, it

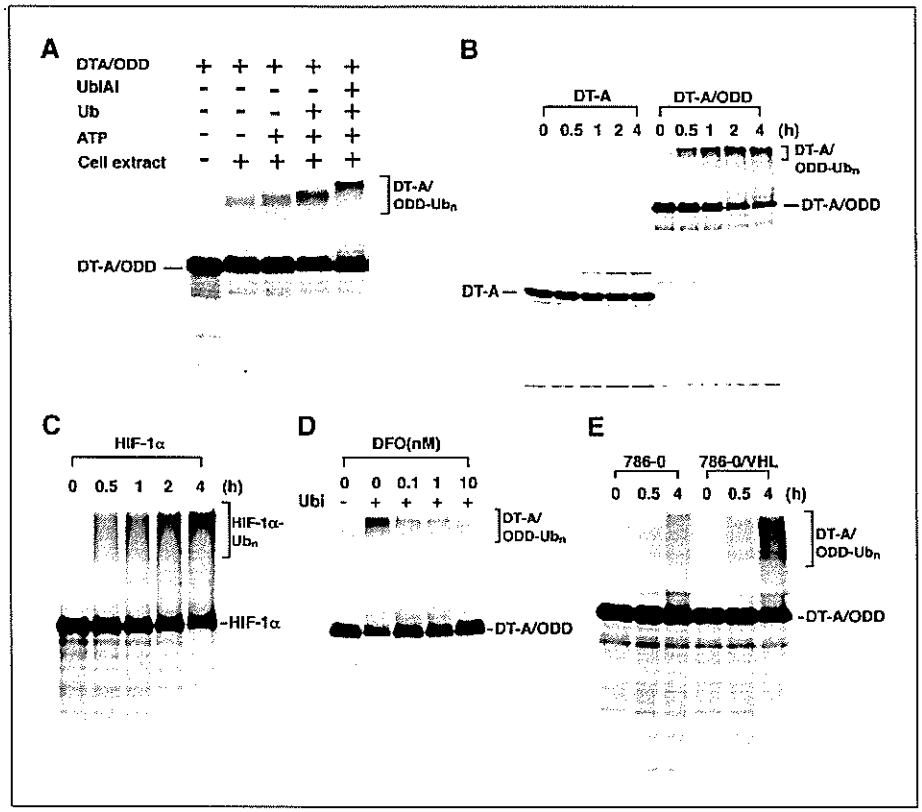

Figure 1. Oxygen- and pVHL-dependent ubiquitination of DT-A/ODD. *A, in vitro* ubiquitination of DT-A/ODD. ^{35}S-labeled DT-A/ODD was subjected to *in vitro* ubiquitination in reactions of different composition. Additions are indicated as follows: 293T S100 fraction (*cell extract*), ATP-regenerating system (*ATP*), ubiquitin (*Ub*), and ubiquitin aldehyde (*UbAl*). The mixture was incubated for 4 hours at 30°C. *B*, time course of ubiquitination of DT-A and DT-A/ODD proteins. ^{35}S-labeled DT-A and DT-A/ODD proteins were subjected to *in vitro* ubiquitination in reactions containing all components described above. *C*, ubiquitination of HIF-1α. ^{35}S-labeled HIF-1α was subjected to *in vitro* ubiquitination assay as in (*B*) for the indicated period. *D*, oxygen-dependent ubiquitination of DT-A/ODD. ^{35}S-labeled DT-A/ODD was subjected to *in vitro* ubiquitination assay in the presence or absence of ubiquitin. The mixture was incubated for 4 hours in the presence of the indicated concentrations of desferrioxamine (*DFO*). *E*, pVHL-dependent ubiquitination of DT-A/ODD. ^{35}S-labeled DT-A/ODD was subjected to *in vitro* ubiquitination assay as in (*B*) for the indicated period, except using S100 fraction prepared from 786-O or 786-O/VHL cells.

greatly enhanced the activity under hypoxic conditions in both cells. Similar results were obtained in human mammary carcinoma MCF7 cells and human foreskin fibroblasts (data not shown). Thus, EBBS caused a marked enhancement in luciferase activity in different cell types in hypoxia probably due to its mRNA-stabilizing effect.

***In vitro* protein synthesis inhibition by diphtheria toxin A, DT-A/ODD, and its attenuated fusion proteins.** We next examined whether fusion of HIF-1α ODD domain to DT-A affects the translation inhibitory activity of DT-A. For this, we first made *in vitro* translated DT-A and DT-A/ODD and then added them to the *in vitro* luciferase gene transcription/translation system with or without exogenously added NAD$^+$. Figure 3 shows the amount of translated ^{35}S-labeled luciferase protein. DT-A significantly reduced the level of luciferase protein even in the absence of exogenous NAD$^+$ and nearly completely inhibited the translation in the presence of NAD$^+$. DT-A/ODD was comparable with DT-A in inhibiting translation. We also made attenuated DT-A/ODD proteins, DT-A^{W153F}/ODD and DT-A^{H21A}/ODD, and measured their translation inhibitory activities in a similar way. DT-A^{W153F} and DT-A^{H21A} have been reported to have about a 4-fold and 120-fold reduced ADP ribosyltransferase activity compared with DT-A, respectively (40, 41). Consistent with the reports, DT-A^{W153F}/ODD was less effective in inhibiting the synthesis of luciferase protein compared with DT-A/ODD. DT-A^{H21A}/ODD exhibited the least inhibitory activity.

Induction of apoptosis by DT-A/ODD proteins in A11 cells under hypoxic conditions. Based on the above results, we constructed DT-A expression plasmids, pVEGFpro-DT-A/ODD-EBBS, pVEGFpro-DT-A^{W153F}/ODD-EBBS, and pVEGFpro-DT-A^{H21A}/ODD-EBBS. To investigate the effect of these expression plasmids on apoptosis of A11 cells under normoxic and hypoxic conditions, we transfected each of them into A11 cells, cultured the cells under normoxic or hypoxic conditions for 24 hours, and then stained them for Annexin V. The transfection efficiency was 20% to 30% as assessed by pEGFP-N1 expression vector. As shown in Fig. 4*A*, hypoxia alone did not induce apoptosis in the control

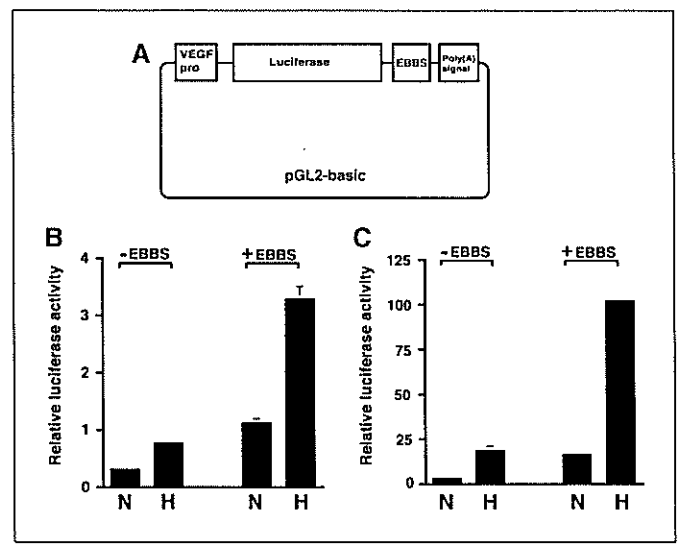

Figure 2. Effect of EBBS on the expression level of a heterologous gene under hypoxic conditions. *A*, schematic representation of the luciferase reporter constructs. *VEGFpro*, VEGF gene promoter. *B* and *C*, effect of EBBS on the expression level of a luciferase reporter gene. A11 or HepG2 cells cotransfected with pVEGFpro-Luc or pVEGFpro-Luc-EBBS and pRL-CMV as an internal control were cultured for 18 hours under normoxic (*N*) or hypoxic (*H*) conditions. All luciferase activities were normalized for transfection efficiency and background luciferase activities obtained from cells transfected with a promoterless luciferase gene *pGL2-basic* were subtracted from this value. *Columns*, luciferase activity expressed in arbitrary units; *bars*, SD of triplicate determinations.

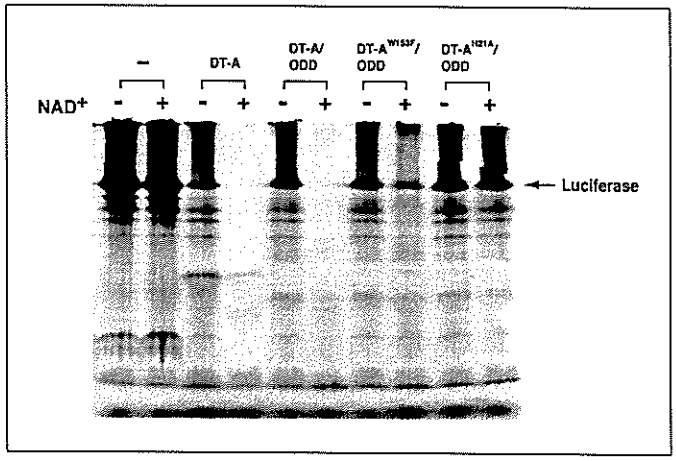

Figure 3. *In vitro* protein synthesis inhibitory activity of wild-type and attenuated DT-A/ODD fusion protein. DT-A/ODD, DT-A^{W153F}/ODD, or DT-A^{H21A}/ODD prepared by TNT T7 Quick Coupled Transcription/Translation System was added to TNT SP6 Quick Coupled Transcription/Translation mixture composed of [^{35}S]PRO-MIX and luciferase SP6 control DNA. The reaction mixtures were incubated for 90 minutes at 30°C in the presence or absence of NAD$^+$. Newly synthesized luciferase protein was separated on SDS-PAGE and detected by autoradiography.

plasmid-transfected cells, thus excluding nonspecific induction of apoptosis. The reason why ~10% of Annexin V–positive cells were observed in the control plasmid-transfected cells is unknown; however, it may be due to the toxicity of the transfection reagent. Expression of DT-A/ODD proteins resulted in a significant increase in the number of Annexin V–positive cells irrespective of oxygen tension. Expression of DT-A^{W153F}/ODD or DT-A^{H21A}/ODD did not apparently induce apoptosis under normoxic conditions. In contrast, they significantly caused an increase in the number of Annexin V–positive cells under hypoxic conditions, DT-A^{W153F}/ODD being more potent than DT-A^{H21A}/ODD (Fig. 4*A* and *B*). Similar results were obtained in their abilities to induce sub-G_1 fraction, another criteria of apoptosis, under hypoxic conditions (Fig. 4*C*). Long-term exposure of A11 cells to severe hypoxia resulted in cell death to some extent, but expression of DT-A^{W153F}/ODD further enhanced cell death (Fig. 4*D*). Thus, transfection of pVEGFpro-DT-A^{W153F}/ODD-EBBS or pVEGFpro-DT-A^{H21A}/ODD-EBBS plasmid into A11 cells led to a clear hypoxia-dependent induction of apoptosis.

Establishment of A11H10 cells with higher resistance to hypoxia-induced apoptosis. We next wanted to investigate the effect of liposomal gene transfer of the DT-A/ODD expression construct on induction of apoptosis in hypoxic regions of tumors. Before this experiment, we established A11H10 cells with higher resistance to hypoxia-induced apoptosis than A11 cells and used them as target cells. The cells were actually more resistant to apoptosis induced by severe hypoxia (<0.1% O_2) than A11 cells (Fig. 5*A*) and survived for >5 days in severe hypoxia (Fig. 5*B*). They were also more resistant to apoptosis triggered by an anticancer drug cisplatin than A11 cells (Fig. 5*C*). The apoptosis-resistant phenotype was stable at least for 3 months (data not shown). A11H10 cells expressed VEGF mRNA as well as A11 cells in response to hypoxia (Fig. 5*D*).

Apoptosis induction by liposomal transfer of diphtheria toxin A expression plasmid in hypoxic regions of A11H10 tumors. From the results described above, we chose the pVEGFpro-DT-A^{W153F}/ODD-EBBS expression construct and examined its effect on apoptosis induction in tumors. Before this experiment, we directly injected pEGFP-N1/DIMRIE-C complex in A11H10 tumors along with lysine-fixable dextran-TMR to see if we can use dextran-TMR for later identification of injected areas. Two days after the injection, tumors were surgically removed and cryosections were prepared. Observation of the specimen revealed that EGFP-expressing tumor cells located in dextran-TMR–positive areas, indicating that dextran-TMR can be used to identify injected areas (Fig. 6). We then intratumorally injected pVEGFpro or pVEGFpro-DT-A^{W153F}/ODD-EBBS/DMRIE-C complex together with

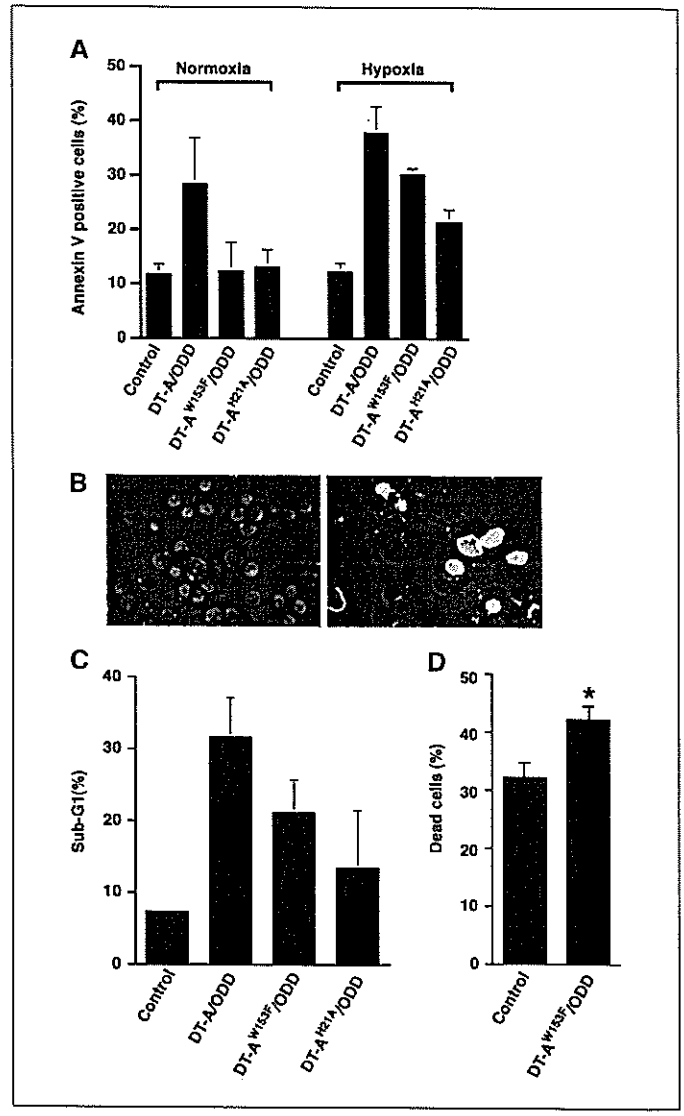

Figure 4. Induction of apoptosis in A11 cells transfected with pVEGFpro-DT-A/ODD-EBBS, pVEGFpro-DT-A^{W153F}/ODD-EBBS, and pVEGFpro-DT-A^{H21A}/ODD-EBBS vectors. A11 cells were transiently transfected with pVEGFpro as a control, pVEGFpro-DT-A/ODD-EBBS, pVEGFpro-DT-A^{W153F}/ODD-EBBS, and pVEGFpro-DT-A^{H21A}/ODD-EBBS. After culturing the cells under normoxic or hypoxic conditions for 24, 36, or 48 hours, the cells were processed for Annexin V staining (*A* and *B*), sub-G_1 analysis (*C*), or trypan blue dye exclusion test (*D*), respectively. *A*, induction of Annexin V–positive cells by the expression vectors. *B*, Annexin V–positive cells induced by the transfection of pVEGFpro-DT-A^{W153F}/ODD-EBBS in normoxia (*left*) or hypoxia (*right*). The fluorescence was observed under a confocal laser microscope. *C*, induction of cellular DNA fragmentation (sub-G_1) by the expression vectors in hypoxia. *Columns*, percentage of sub-G_1 fraction determined with a FACScan flow cytometer. *D*, induction of cell death by the expression vectors in severe hypoxia. *Columns*, percentage of dead cells; *bars*, SD of triplicate determinations. *, $P < 0.007$.

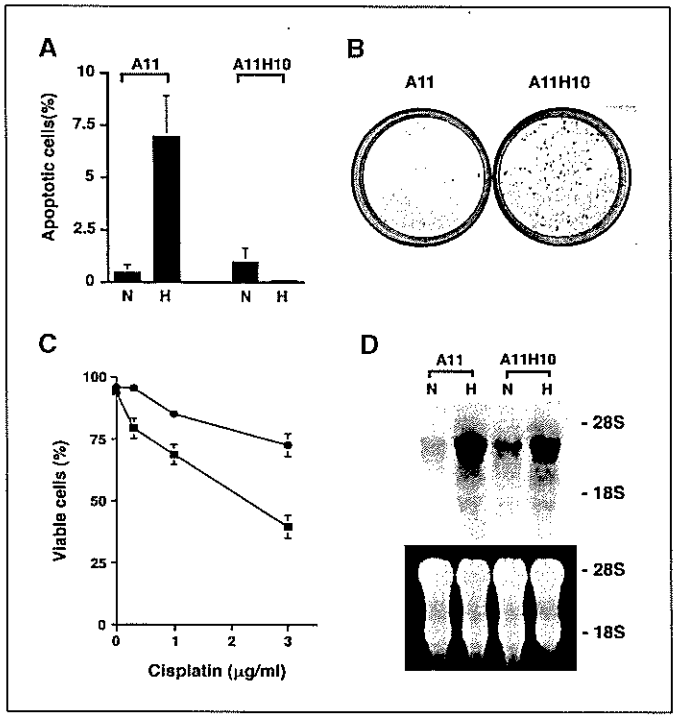

Figure 5. Establishment and characterization of A11H10 cells. *A*, apoptosis of A11 and A11H10 cells in severe hypoxia. The cells were cultured in normoxia or severe hypoxia (<0.1% O_2; *H*) for 28 hours and the percentage of cells with chromatin condensation and fragmentation was determined after DAPI staining. *Columns*, percentage of apoptotic cells; *bars*, SD of triplicate determinations. *B*, survival of A11 and A11H10 cells in severe hypoxia. The cells (1×10^5) were cultured in severe hypoxia (<0.1% O_2) for 5 days followed by culturing in normoxia for 7 days. Colonies were stained with crystal violet. *C*, sensitivity of A11 and A11H10 cells to cisplatin. The cells were exposed to the indicated concentrations of cisplatin for 2 days. Cell viability was assessed by trypan blue dye exclusion. *Points*, percentage of viable cells; *bars*, SD of triplicate determinations. *D*, *VEGF* mRNA expression in A11 and A11H10 cells. Total RNA was isolated from the cells cultured in normoxia or hypoxia for 8 hours and subjected to Northern analysis. Blots were hybridized with ^{32}P-labeled mouse *VEGF* cDNA. Ethidium bromide staining of the gel is also shown.

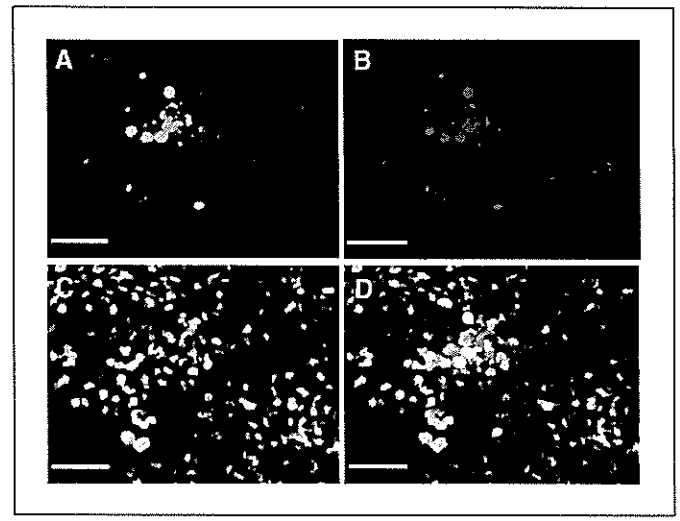

Figure 6. Liposomal gene transfer of pEGFP-N1 into A11H10 tumors. pEGFP-N1/DMRIE-C complex was directly injected into s.c. A11H10 tumors along with dextran-TMR. Two days after the injection, cryosections were prepared, stained with Hoechst 33342, and then observed under a fluorescent microscope for EGFP (*green*), dextran-TMR (*orange*), and Hoechst 33342 (*blue*). Images were captured using a Cool SNAP charge-coupled device camera and pseudocolored by a RS IMAGE Express image processing software. *A*, EGFP. *B*, dextran-TMR. *C*, Hoechst33342. *D*, merged. Note that EGFP-expressing cells locate in dextran-TMR-positive areas. Bar, 50 μm.

dextran-TMR, and 2 days after the injection we administered EF5 for discrimination between normoxic and hypoxic regions. Cryosections were prepared and processed for TUNEL staining followed by staining with Cy5-labeled anti-EF5 antibody and Hoechst staining. We omitted necrotic areas from the analyses. The results showed that a few TUNEL-positive cells were observed in dextran-TMR–negative areas of both control and pVEGFpro-DT-A^{W153F}/ODD-EBBS plasmid-injected tumors (Fig. 7*A* and *C*), whereas a large number of TUNEL-positive cells were detected in dextran-TMR-positive areas of the pVEGFpro-DT-A^{W153F}/ODD-EBBS-injected tumors (Fig. 7*D*) but not of the pVEGFpro-injected tumors (Fig. 7*B*). Closer observations of the specimen of the pVEGFpro-DT-A^{W153F}/ODD-EBBS-injected tumors revealed that only a small number of TUNEL-positive cells were evident in dextran-TMR–positive and EF5-negative (normoxic) areas (Fig. 8*A-D*), whereas a large number of TUNEL-positive cells were detected in dextran-TMR-positive and EF5-positive (hypoxic) areas (Fig. 8*E-H*). Thus, these results indicate that apoptosis was remarkably induced by liposomal transfer of pVEGF-DT-A^{W153F}/ODD-EBBS expression construct in hypoxic, but not in normoxic, regions of A11H10 tumors.

Tumor growth inhibition by liposomal transfer of diphtheria toxin A expression plasmi d in P29 tumors. Based on the above results, we repeatedly injected pVEGF-DT-A^{W153F}/ODD-EBBS/liposome complex into A11H10 tumors to see the therapeutic effect of the plasmid. However, the inhibition of tumor growth was marginal (data not shown). We speculated that this is due to the fact that A11 tumors are well vascularized (42) and, hence, not so hypoxic. We then used P29 tumors because they are poorly vascularized (42). Actually, as expected, EF5 staining showed that P29 tumors contained increased hypoxic areas compared with A11H10 tumors (Fig. 9*A* and *B*). We therefore examined the effect

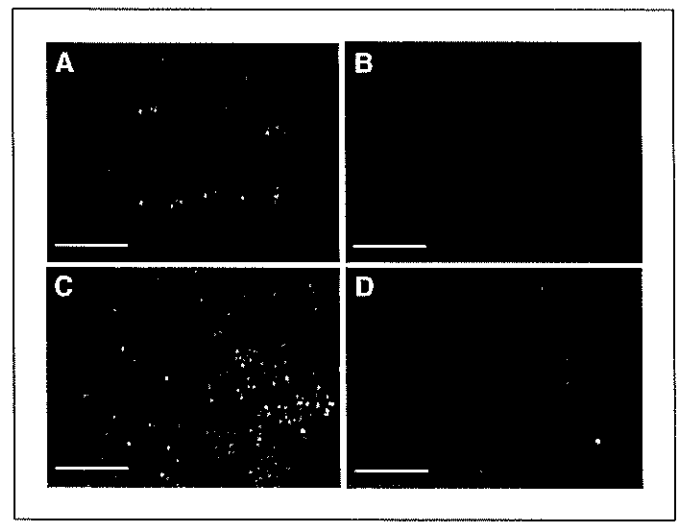

Figure 7. Apoptosis induction by liposomal gene transfer of pVEGFpro-DT-A^{W153F}/ODD-EBBS into A11H10 tumors. pVEGFpro as a control (*A* and *B*) or pVEGFpro-DT-A^{W153F}/ODD-EBBS/DMRIE-C complex (*C* and *D*) was directly injected into A11H10 tumors along with dextran-TMR. Two days after the injection, cryosections were prepared, stained for TUNEL, and observed under a confocal microscope for TUNEL-positive cells (*green*) and dextran-TMR (*orange*). *A* and *C*, dextran-TMR–positive areas. *B* and *D*, dextran-TMR–negative areas. Bar, 100 μm.

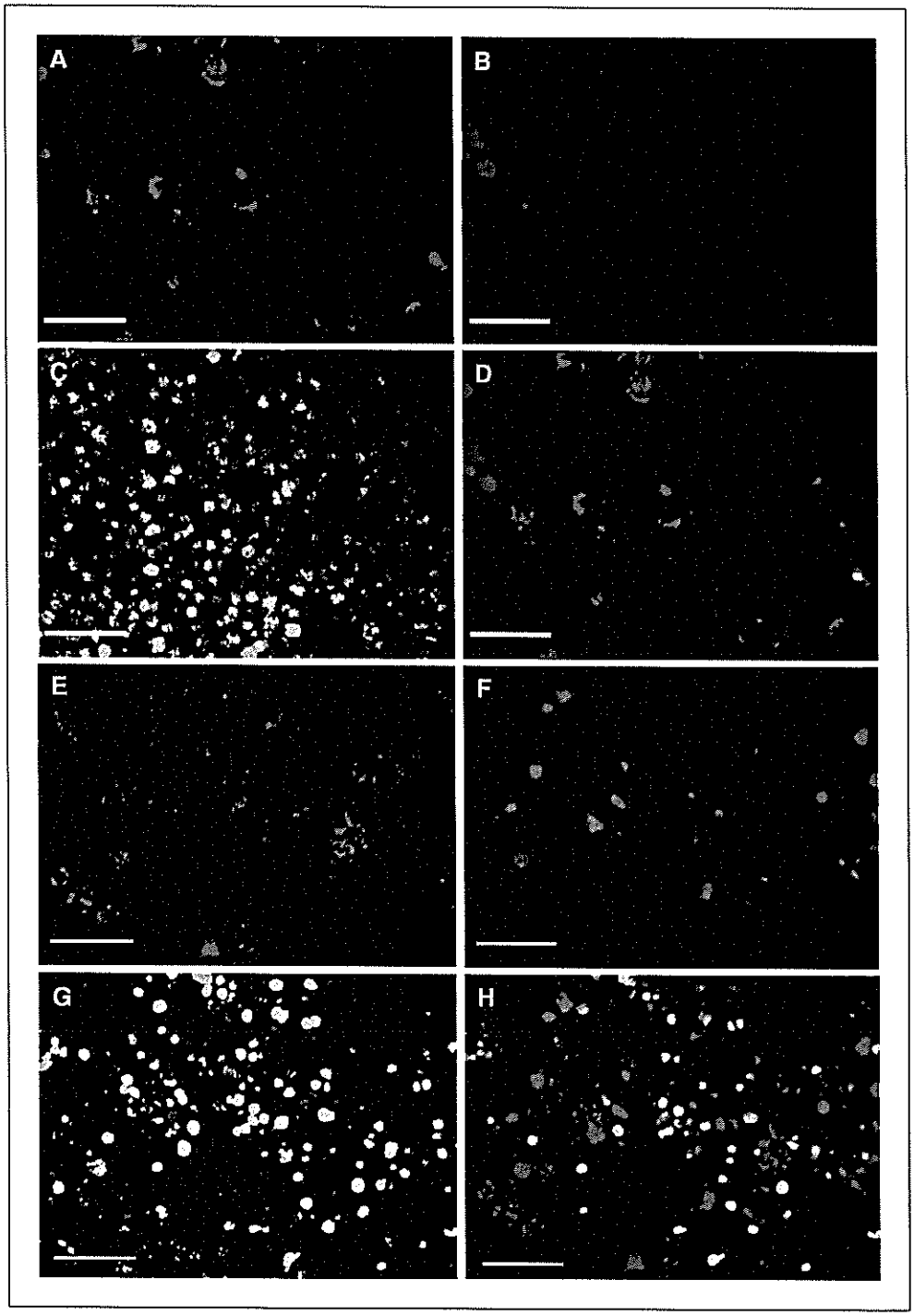

Figure 8. Apoptosis induction in hypoxic areas of A11H10 tumors after liposomal gene transfer of pVEGFpro-DT-A^{W153F}/ODD-EBBS. pVEGFpro-DT-A^{W153F}/ODD-EBBS/DMRIE-C complex was directly injected into A11H10 tumors along with dextran-TMR. Two days after the injection, the mice were administered with EF5. The cryosections of tumors were successively processed for TUNEL, EF5, and Hoechst 33342 stainings. Images were captured using a Cool SNAP charge-coupled device camera and pseudocolored by a RS IMAGE Express image processing software. TUNEL (*green*), EF5 (*pink*), Hoechst 33342 (*blue*), and dextran-TMR (*orange*). *A* to *D*, dextran-TMR–positive and EF5-negative areas. *E* to *H*, dextran-TMR–positive and EF5-positive areas. *A* and *E*, dextran-TMR. *B* and *F*, EF5. *C* and *G*, merged image of TUNEL and Hoechst 33342. *D* and *H*, merged image of TUNEL, EF5, and dextran-TMR. Bar, 50 μm.

of multiple injections of the expression construct on P29 tumor growth. The results showed that a modest but statistically significant growth inhibition was observed in the mice with pVEGF-DT-A^{W153F}/ODD-EBBS compared with the mice with pVEGFpro without apparent side effects, such as body weight loss (Fig. 10*A* and *B*).

Discussion

In this study, we examined the effectiveness of VEGF promoter–driven DT-A expression for killing hypoxic tumor cells. To reduce cytotoxicity of DT-A in normal cells and increase hypoxia specificity, we constructed the expression vector to express DT-A/ODD fusion protein to produce mRNA containing the EBBS and not to include unnecessary enhancer/promoter sequence other than VEGF promoter. The results showed that DT-A/ODD, but not DT-A, was ubiquitinated as well as HIF-1α in a pVHL- and oxygen-dependent manner in *in vitro* ubiquitination assays. The EBBS exhibited mRNA-stabilizing effect, as shown by luciferase reporter assays. Thus, HIF-1α ODD domain and the EBBS worked accordingly. In addition, DT-A/ODD exhibited a comparable inhibitory activity of protein synthesis with DT-A *in vitro*, indicating that fusion of the ODD domain to DT-A does not affect its translation inhibitory activity.

The ODD domain of HIF-1α has been implicated to be useful as a hypoxia switch, limiting the production of a fusion protein in normoxia while stabilizing it in hypoxia (43). For example, ODD–caspase-3 fusion protein is shown to be specifically stabilized and activated in hypoxic cells (44). The present study also showed that the ODD domain is capable of regulating the toxicity of attenuated DT-A, probably rendering the fusion protein to be recognized by pVHL and subsequently degraded through proteasome pathway. However, we presently have no evidence that these events actually occur in the cells.

ERBP was initially identified as the protein(s) that specifically binds to a 120 base fragment (EBBS) of the 3′ UTR of *Epo* mRNA. ERBP binds to this sequence and prolongs the half-life of *Epo* mRNA as well as other reporter mRNA containing EBBS in normoxia and further in hypoxia (23). Although Epo is mainly expressed in cells derived from the liver and the kidney, ERBP is present in other tissues, such as lung, brain, and spleen (23). We could also observe the reporter mRNA-stabilizing effect of EBBS in lung carcinoma cells, hepatoma cells, breast carcinoma cells, and fibroblasts. Therefore, EBBS is able to stabilize a heterologous transcript in a variety of cell types. An alternative to stabilize mRNA in hypoxia may be the use of HuR-binding sequence or recently identified PAIP2-binding sequence, both of which are present in *VEGF* mRNA (22, 45). These elements could substitute for the EBBS in the present expression vector.

Transfection of pVEGFpro-DT-A/ODD-EBBS expression vector into high-metastatic A11 cells resulted in a marked induction of apoptosis in both normoxia and hypoxia. This indicated that only a background expression level of DT-A/ODD is too cytotoxic to be regulated. We then sought to use attenuated DT-A/ODD, DT-A^{W153F}/ODD, and DT-A^{H21A}/ODD, expecting that although they are less active in inhibiting protein synthesis than DT-A/ODD under normoxic conditions, they may exhibit a significantly higher activity when expressed and accumulated in the cells under hypoxic conditions. The results showed that DT-A^{W153F}/ODD and DT-A^{H21A}/ODD were very weak in inducing apoptosis under normoxic conditions, whereas they significantly induced apoptosis under hypoxic conditions. Thus, we could observe hypoxia-dependent induction of apoptosis in A11 cells transfected with the attenuated DT-A/ODD expression vector. The pVEGFpro-DT-A^{W153F}/ODD-EBBS was superior to pVEGFpro-DT-A^{H21A}/ODD-EBBS in inducing apoptosis.

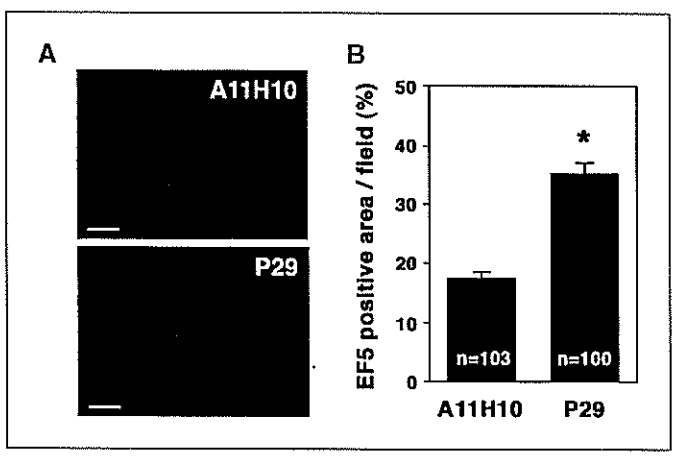

Figure 9. The degree of intratumoral hypoxia in A11H10 and P29 tumors. *A*, detection of hypoxic areas in tumors by EF5 staining. Frozen sections of s.c. tumor established from A11H10 and P29 cells were stained for EF5. Bar, 100 μm. *B*, the degree of hypoxia in A11H10 and P29 tumors. Frozen sections prepared from different regions of A11H10 and P29 tumor were stained for EF5. The fluorescent images of >100 fields (1.175 mm^2/field) were analyzed and the percentage of EF5-positive area per field (*columns*) was calculated. *Bars*, SE. *, $P < 0.0001$.

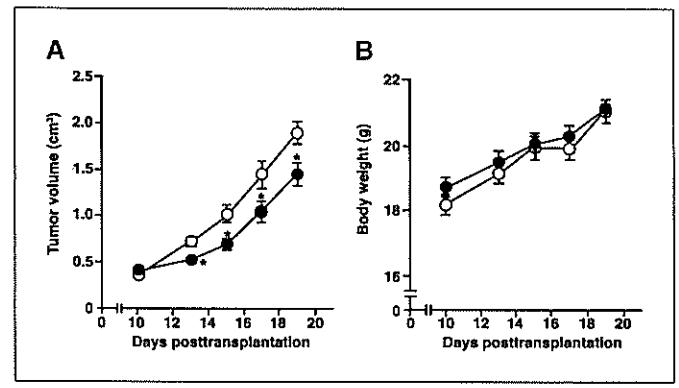

Figure 10. Growth inhibition of P29 tumors by liposomal gene transfer of pVEGFpro-DT-A^{W153F}/ODD-EBBS. *A*, growth of tumors injected with pVEGFpro (○) or pVEGFpro-DT-A^{W153F}/ODD-EBBS/DMRIE-C complex (●). The liposome complex was directly injected into the tumor daily. *B*, body weight of the mice with pVEGFpro (○) or pVEGFpro-DT-A^{W153F}/ODD-EBBS (●). *Bars*, SE. *, $P < 0.04$.

Given that the pVEGFpro-DT-A^{W153F}/ODD-EBBS vector strongly induce apoptosis in the transfected cells under hypoxic but not normoxic conditions, we decided to apply pVEGFpro-DT-A^{W153F}/ODD-EBBS vector to *in vivo* experiments. Before investigating the effect, we established A11H10 cells that are highly resistant to hypoxia-induced apoptosis. We previously reported that A11 cells are more resistant to apoptosis induced by microenvironmental stresses than low-metastatic counterparts (8). A11H10 cells were further more resistant than A11 cells to not only hypoxia but also anticancer drugs and various ER stresses (glucose deprivation, tunicamycin, brefeldin A, calcium ionophore A23187; data not shown). Therefore, the cells enabled us to examine the effect of the expression vector on the tumors that are more difficult to cure. After establishing s.c. A11H10 tumors, we directly injected pVEGFpro-EBBS/liposome complex as a control or pVEGFpro-DT-A^{W153F}/ODD-EBBS/liposome complex with dextran-TMR conjugates, which are frequently used for long-term tracers of live cells. Dextran-TMR conjugates were not toxic and could be detected in the tumors at least 3 days after the injection (data not shown) and, therefore, it was useful to monitor the injection areas of DNA/liposome complex. Actually, EGFP was expressed in cells located in dextran-TMR–positive areas in the tumors administrated with pEGFP-N1 plasmid/DMRIE-C complex. To detect hypoxic areas in the tumors, we used EF5, a derivative of nitroimidazole (39). The results showed that pVEGFpro-EBBS/liposome administration hardly induced apoptotic (TUNEL-positive) cells in dextran-TMR–positive areas. In contrast, pVEGFpro-DT-A^{W153F}/ODD-EBBS/liposome administration resulted in a striking induction of apoptosis in dextran-TMR–positive areas. More specifically, apoptotic cells were detected in hypoxic, but not in normoxic, areas of pVEGFpro-DT-A^{W153F}/ODD-EBBS/liposome-administered tumors. These results clearly indicate that intratumoral injection of pVEGFpro-DT-A^{W153F}/ODD-EBBS/liposome complex induced apoptosis in a hypoxia-dependent fashion. It should be noted, however, that we could not observe a clear tumor growth inhibition after multiple injection of pVEGFpro-DT-A^{W153F}/ODD-EBBS/liposome complex into a tumor mass. This contrasts to the case of direct injection of α-fetoprotein promoter/

enhancer-driven DT-A expression construct/DMRIE-C complex into hepatoma in which significant growth retardation was observed (33). However, our results rather seem to reflect the hypoxia specificity of our expression construct. Because total hypoxic areas in an A11H10 tumor mass are small relative to total normoxic areas, an obvious growth inhibition may not be observed even if all hypoxic tumor cells are killed. Then, to test the therapeutic effect of the expression vector in more hypoxic tumors, we chose P29 tumors that have poorer vasculature and, thus, are more hypoxic than A11 tumors. As a result, we could clearly observe growth retardation of the tumor. Although the effect was not so striking, it may be due to the hypoxia specificity and inefficient *in vivo* gene transfer.

The present DT-A^{W153F}/ODD expression vector would be applicable to a wide variety of tumors, especially those with severe hypoxia, such as cervical cancer and melanomas (46). These cancers are also suitable for intratumoral gene delivery. A critical point to be improved in the future is the transfection method of the vector into hypoxic tumor cells. Although liposomes used here have many advantages as a gene transfer method, such as low evocation of inflammations and immune responses, transfection efficiency is not so high. A solution to this point may be the use of adenoviruses and recently developed DT-resistant packaging line (34), which may allow us to produce a high titer of adenoviruses encoding DT-A^{W153F}/ODD. Combination of such adenoviruses and conventional therapeutic regimens may lead to total killing of tumor cells and ultimately prevention of tumor recurrence.

Acknowledgments

Received 1/13/2005; revised 8/24/2005; accepted 9/30/2005.

Grant support: Grant-in-aid from the Ministry of Health, Labour, and Welfare for Third Term Comprehensive Control Research for Cancer.

The costs of publication of this article were defrayed in part by the payment of page charges. This article must therefore be hereby marked *advertisement* in accordance with 18 U.S.C. Section 1734 solely to indicate this fact.

We thank Dr. S. Fujimoto for his support.

References

1. Brown JM, Giaccia AJ. The unique physiology of solid tumors: opportunities (and problems) for cancer therapy. Cancer Res 1998;58:1408–16.
2. Chaplin DJ, Hill SA. Temporal heterogeneity in microregional erythrocyte flux in experimental solid tumours. Br J Cancer 1995;71:1210–3.
3. Teicher BA. Hypoxia and drug resistance. Cancer Metastasis Rev 1994;13:139–68.
4. Cairns RA, Kalliomaki T, Hill RP. Acute (cyclic) hypoxia enhances spontaneous metastasis of KHT murine tumors. Cancer Res 2001;61:8903–8.
5. Pennacchietti S, Michieli P, Galluzzo M, et al. Hypoxia promotes invasive growth by transcriptional activation of the met protooncogene. Cancer Cell 2003;3:347–61.
6. Staller P, Sulitkova J, Lisztwan J, et al. Chemokine receptor CXCR4 downregulated by von Hippel-Lindau tumour suppressor pVHL. Nature 2003;425:307–11.
7. Graeber TG, Osmanian C, Jacks T, et al. Hypoxia-mediated selection of cells with diminished apoptotic potential in solid tumours. Nature 1996;379:88–91.
8. Takasu M, Tada Y, Wang JO, Tagawa M, Takenaga K. Resistance to apoptosis induced by microenvironmental stresses is correlated with metastatic potential in Lewis lung carcinoma. Clin Exp Metastasis 1999;17:409–16.
9. Rice GC, Hoy C, Schimke RT. Transient hypoxia enhances the frequency of dihydrofolate reductase gene amplification in Chinese hamster ovary cells. Proc Natl Acad Sci U S A 1986;83:5978–82.
10. Russo CA, Weber TK, Volpe CM, et al. An anoxia inducible endonuclease and enhanced DNA breakage as contributors to genomic instability in cancer. Cancer Res 1995;55:1122–8.
11. Coquelle A, Toledo F, Stern S, Bieth A, Debatisse M. A new role for hypoxia in tumor progression: induction of fragile site triggering genomic rearrangements and formation of complex DMs and HSRs. Mol Cell 1998;2:259–65.
12. Goldberg MA, Schneider TJ. Similarities between the oxygen-sensing mechanisms regulating the expression of vascular endothelial growth factor and erythropoietin. J Biol Chem 1994;269:4355–9.
13. Goldberg MA, Glass GA, Cunningham JM, Bunn HF. The regulated expression of erythropoietin by two human hepatoma cell lines. Proc Natl Acad Sci U S A 1987;84:7972–6.
14. Ikeda E, Achen MG, Breier G, Risau W. Hypoxia-induced transcriptional activation and increased mRNA stability of vascular endothelial growth factor in C6 glioma cells. J Biol Chem 1995;270:19761–6.
15. Wenger RH, Gassmann M. Oxygen(s) and the hypoxia-inducible factor-1. Biol Chem 1997;378:609–16.
16. Hofer T, Wenger H, Gassmann M. Oxygen sensing, HIF-1α stabilization and potential therapeutic strategies. Pflugers Arch 2002;443:503–7.
17. Forsythe JA, Jiang BH, Iyer NV, et al. Activation of vascular endothelial growth factor gene transcription by hypoxia-inducible factor 1. Mol Cell Biol 1996;16:4604–13.
18. Maxwell PH, Wiesener MS, Chang GW, et al. The tumour suppressor protein VHL targets hypoxia-inducible factors for oxygen-dependent proteolysis. Nature 1999;399:271–5.
19. Ivan M, Kaelin WG, Jr. The von Hippel-Lindau tumor suppressor protein. Curr Opin Genet Dev 2001;11:27–34.
20. Jaakkola P, Mole DR, Tian YM, et al. Targeting of HIF-α to the von Hippel-Lindau ubiquitylation complex by O_2-regulated prolyl hydroxylation. Science 2001;292:468–72.
21. Jewell UR, Kvietikova I, Scheid A, et al. Induction of HIF-1α in response to hypoxia is instantaneous. FASEB J 2001;15:1312–4.
22. Goldberg-Cohen I, Furneauxb H, Levy AP. A 40-bp RNA element that mediates stabilization of vascular endothelial growth factor mRNA by HuR. J Biol Chem 2002;277:13635–40.
23. McGary EC, Rondon IJ, Beckman BS. Post-transcriptional regulation of erythropoietin mRNA stability by erythropoietin mRNA-binding protein. J Biol Chem 1997;272:8628–34.
24. Dachs GU, Patterson AV, Firth JD, et al. Targeting gene expression to hypoxic tumor cells. Nat Med 1997;3:515–20.
25. Koshikawa N, Takenaga K, Tagawa M, Sakiyama S. Therapeutic efficacy of the suicide gene driven by the promoter of vascular endothelial growth factor gene against hypoxic tumor cells. Cancer Res 2000;60:2936–41.
26. Harris AL. Hypoxia—a key regulatory factor in tumour growth. Nat Rev Cancer 2002;2:38–47.
27. Binley K, Askham Z, Martin L, et al. Hypoxia-mediated tumour targeting. Gene Ther 2003;10:540–9.
28. Collier RJ. Diphtheria toxin: mode of action and structure. Bacteriol Rev 1975;39:54–85.
29. Vingerhoeds MH, Steerenberg PA, Hendriks JJ, et al. Targeted delivery of diphtheria toxin via immunoliposomes: efficient antitumor activity in the presence of inactivating anti-diphtheria toxin antibodies. FEBS Lett 1996;395:245–50.
30. Kreitman RJ. Immunotoxins in cancer therapy. Curr Opin Immunol 1999;11:570–8.
31. Maxwell IH, Maxwell F, Glode LM. Regulated expression of a diphtheria toxin A-chain gene transfected into human cells: possible strategy for inducing cancer cell suicide. Cancer Res 1986;46:4660–4.
32. Hall PD, Willingham MC, Kreitman RJ, Frankel AE. DT388-GM-CSF, a novel fusion toxin consisting of a truncated diphtheria toxin fused to human granulocyte-macrophage colony-stimulating factor, prolongs host survival in a SCID mouse model of acute myeloid leukemia. Leukemia 1999;13:629–33.
33. Kunitomi M, Takayama E, Suzuki S, et al. Selective inhibition of hepatoma cells using diphtheria toxin A under the control of the promoter/enhancer region of the human α-fetoprotein gene. Jpn J Cancer Res 2000;91:343–50.
34. Li Y, McCadden J, Ferrer F, et al. Prostate-specific expression of the diphtheria toxin A chain (DT-A): studies of inducibility and specificity of expression of prostate-specific antigen promoter-driven DT-A adenoviral-mediated gene transfer. Cancer Res 2002;62:2576–82.
35. Keyvani K, Baur I, Paulus W. Tetracyclin-controlled expression but not toxicity of an attenuated diphtheria toxin mutant. Life Sci 1999;64:1719–24.
36. Kimura H, Weisz A, Kurashima Y, et al. Hypoxia response element of the human vascular endothelial growth factor gene mediates transcriptional regulation by nitric oxide: control of hypoxia-inducible factor-1 activity by nitric oxide. Blood 2000;95:189–97.
37. Cockman ME, Masson N, Mole DR, et al. Hypoxia inducible factor-α binding and ubiquitylation by the von Hippel-Lindau tumor suppressor protein. J Biol Chem 2000;275:25733–41.
38. Epinat J-C, Gilmore TD. *In vitro*-translated diphtheria toxin A chain inhibits translation in wheat germ extracts: analysis of biologically active, caspase-3-resistant diphtheria toxin mutants. Biochim Biophys Acta 1999;1472:34–41.
39. Lord EM, Harwell L, Koch CJ. Detection of hypoxic cells by monoclonal antibody recognizing 2-nitroimidazole adducts. Cancer Res 1993;53:5721–6.
40. Zdanovskaia MV, Zdanovsky AG, Yankovsky NK. Diphtheria toxin NAD affinity and ADP ribosyltransferase activity are reduced at tryptophan 153 substitutions for alanine or phenylalanine. Res Microbiol 2000;151:557–62.
41. Blanke SR, Huang K, Wilson BA, et al. Active-site mutations of the diphtheria toxin catalytic domain: role of histidine-21 in nicotinamide adenine dinucleotide binding and ADP-ribosylation of elongation factor 2. Biochemistry 1994;33:5155–61.
42. Koshikawa N, Iyozumi A, Gassmann M, Takenaga K. Constitutive upregulation of hypoxia-inducible factor-1α mRNA occurring in highly metastatic lung carcinoma cells leads to vascular endothelial growth factor overexpression upon hypoxic exposure. Oncogene 2003;22:6717–24.
43. Payen E, Bettan M, Henri A, et al. Oxygen tension and a pharmacological switch in the regulation of transgene expression for gene therapy. J Gene Med 2001;3:498–504.
44. Harada H, Hiraoka M, Kizaka-Kondoh S. Antitumor effect of TAT-oxygen-dependent degradation-caspase-3 fusion protein specifically stabilized and activated in hypoxic tumor cells. Cancer Res 2002;62:2013–8.
45. Onesto C, Berra E, Grepin R, Pages G. Poly(A) binding protein-interacting protein 2, a strong regulator of vascular endothelial growth factor mRNA. J Biol Chem 2004;279:34217–26.
46. Dachs GU, Tozer GM. Hypoxia-modulated gene expression: angiogenesis, metastasis and therapeutic exploitation. Eur J Cancer 2000;36:1649–60.

Mammalian Polycomb-mediated repression of *Hox* genes requires the essential spliceosomal protein Sf3b1

Kyoichi Isono,[1] Yoko Mizutani-Koseki,[1] Toshihisa Komori,[2] Marion S. Schmidt-Zachmann,[3] and Haruhiko Koseki[1,4]

[1]Developmental Genetics Group, RIKEN Research Center for Allergy and Immunology, Tsurumi-ku, Yokohama 230-0045, Japan; [2]Department of Medicine III, Osaka University Medical School, Suita, Osaka 565-0871, Japan; [3]Division of Cell Biology, German Cancer Research Center, D-69120 Heidelberg, Germany

Polycomb group (PcG) proteins are responsible for the stable repression of homeotic (*Hox*) genes by forming multimeric protein complexes. We show (1) physical interaction between components of the U2 small nuclear ribonucleoprotein particle (U2 snRNP), including Sf3b1 and PcG proteins Zfp144 and Rnf2; and (2) that *Sf3b1*-heterozygous mice exhibit skeletal transformations concomitant with ectopic *Hox* expressions. These alterations are enhanced by *Zfp144* mutation but repressed by *Mll* mutation (a trithorax-group gene). Importantly, the levels of Sf3b1 in PcG complexes were decreased in *Sf3b1*-heterozygous embryos. These findings suggest that Sf3b1–PcG protein interaction is essential for true PcG-mediated repression of *Hox* genes.

Supplemental material is available at http://www.genesdev.org.

Received November 29, 2004; revised version accepted January 14, 2005.

During mammalian development, spatially and quantitatively appropriate homeotic (*Hox*) gene expression is essential for the anterior–posterior specification of axial structures (McGinnis and Krumlauf 1992; Duboule and Morata 1994). The maintenance of the *Hox* gene expressional state is driven by the products of Polycomb group (PcG) and trithorax group (trxG) genes (Satijn and Otte 1999; Francis and Kingston 2001; Simon and Tamkun 2002; Orlando 2003). In general, PcG proteins act as repressors to maintain the silent state, while the trxG proteins are activators that maintain *Hox* gene transcription. PcG proteins constitute large, chromatin-associated multiprotein complexes, which in mammals can be classified into at least two different classes. The Class I complex, which contains Eed/Ezh2, is associated with histone deacetylase and methyltransferase activity. The PRC1 or Class II complex consists of, for example, Zfp144 (Mel18), Rnf2 (Ring1B), Cbx2/M33, and Phc2/Edr2. The Class II complex, which characteristically includes the products from highly related pairs of genes, has been shown to inhibit nucleosome remodeling by the SWI/SNF complex in vitro (Shao et al. 1999). However, as the inhibition requires preincubation of the Class II with the nucleosomal template (it does not occur when Class II and SWI/SNF products are added together), this suggests that the Class II complex does not interact directly with SWI/SNF, but instead competes for the nucleosome template. Possibly, it is this binding of the Class II complex, which prevents nucleosome remodeling, that silences the genes by blocking the access of transcription activators to *cis*-regulatory elements such as promoters and enhancers (Francis et al. 2001). Interestingly, recent studies have proposed an alternative mechanism for maintaining gene silence (Breiling et al. 2001; Saurin et al. 2001). Fly Class II complex includes general transcription factors such as TBP and TBP-associated proteins at promoter regions. Using an in vitro assay, King et al. (2002) showed that the fly complex was able to inhibit transcription by RNA polymerase II at particular steps even after activator binding. This raises the possibility that the Class II complex might act directly on the functioning of the transcriptional machinery. However, whether this silencing mechanism is active at *Hox* loci during mammalian embryo development is not clear. In order to achieve a better understanding of the molecular basis of PcG complex-mediated repressions, we believe that it is important to identify PcG complex-associated non-PcG proteins and subsequently investigate the genetic impact of such proteins on PcG complexes. In this paper, we identified an essential spliceosomal protein Sf3b1 that physically interacts with the Class II PcG proteins and generated *Sf3b1* knockout mice. Surprisingly, *Sf3b1*$^{+/-}$ mice exhibited skeletal phenotypes that are usually observed with *PcG* mutation. Furthermore, genetic interactions between *Sf3b1* and *Zfp144* or the trxG gene *Mll* mutations were also shown. Therefore, it appears that Sf3b1 and the Class II PcG proteins are functionally interacting on the *Hox* loci in developing embryos.

Results and Discussion

Two partial cDNA clones encoding amino acid 1–489 and 312–777 regions of mouse spliceosomal protein Sf3b1 have been isolated as interactors for the mammalian PcG proteins Zfp144 and Rnf2, respectively, by yeast two-hybrid screening (Fig. 1A). Physical interactions between Sf3b1 and PcG proteins were first examined by glutathione S-transferase (GST) pull-down assay. Nuclear proteins were extracted from mouse embryonic stem (ES) cells and subsequently precipitated by GST–Rnf2 and GST–Zfp144 fusion proteins. The precipitates were subjected to immunoblotting with anti-Sf3b1 antibody. Endogenous Sf3b1 was clearly coprecipitated with GST–Rnf2 and GST–Zfp144 (Fig. 1B). Moreover, assay with Rnf2 truncates revealed that Sf3b1 specifically in-

[*Keywords*: *Hox* genes; Polycomb group; knockout mice; spliceosomal proteins]
[4]Corresponding author.
E-MAIL koseki@rcai.riken.jp; FAX 81-45-503-9690.
Article and publication are at http://www.genesdev.org/cgi/doi/10.1101/gad.1284605.

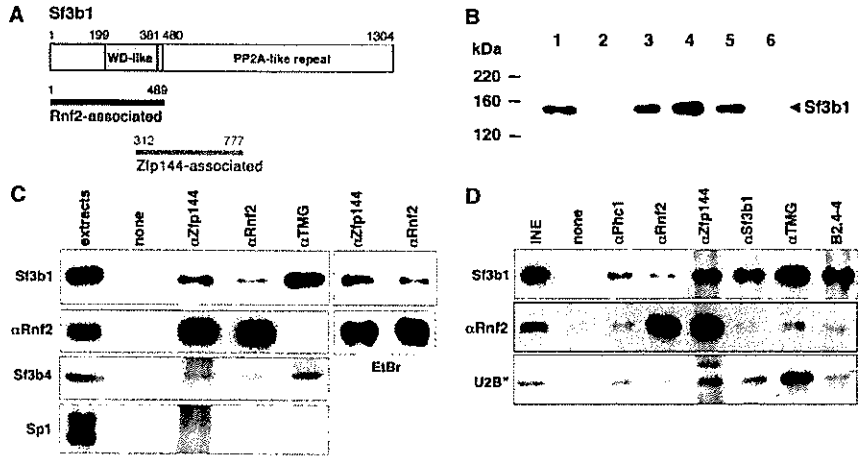

Figure 1. Physical interaction between Sf3b1 and PcG proteins. (*A*) Primary structure of Sf3b1 (Isono et al. 2001). Sf3b1 has WD-40 like repeats and PP2A repeats (usually termed HEAT motifs) originally identified in the PR65 subunit of protein phosphatase 2A. The N-terminal region (amino acids 1–489) and the internal region (amino acids 312–777), respectively, were associated with Rnf2 and Zfp144 in the yeast two-hybrid system. (*B*) GST pull-down assays probed with the Sf3b1-specific antibody. Nuclear extracts from ES cells were incubated with GST alone (lane *2*) and GST fusions with Zfp144 (lane 3), Rnf2 (lane *4*), and the N-terminal (lane *5*) or C-terminal (lane *6*) regions of Rnf2. In lane *1*, one-fifteenth volume of extract sample used in a reaction was applied. (*C*) Coimmunoprecipitation with whole-cell lysates. Lysate of a mouse embryo at 10.75–11.25 dpc was incubated with or without antibodies to Zfp144, Rnf2, or TMG. Each precipitant was divided into two, and each was used in immunoblotting with Sf3b1 and Rnf2 or Sp1 and Sf3b4 antibodies. Anti-Sp1 was used as a negative control. In each "extract" lane, one-fortieth volume of extract sample used in a reaction was applied. In addition, lysates treated with ethidium bromide (EtBr) were also used to exclude DNA. (*D*) Coimmunoprecipitation with chromatin-rich lysates. Insoluble nuclear extract from an embryo at 10.75–11.25 dpc was prepared by osmotic shock, solubilized by sonication, and then incubated with antibodies. Phc1 is a mouse homolog to the fly PcG protein, Polyhomeotic (the fly protein homologous to mouse Phc1). B2.4-4 is a polyclonal antibody against the *Xenopus* Sf3b1, which has an epitope different from the monoclonal antibody (αSf3b1). In the "INE" lane, one-fortieth volume of the insoluble extract used in a reaction was applied.

teracts with the N-terminal region (amino acids 1–188) but not with the C-terminal region (amino acids 189–336). Thus, Sf3b1 probably has the potential to bind directly to Rnf2 and Zfp144.

We examined the in vivo interaction further in whole-cell extracts from 11.5 d post-coitus (dpc) embryos in which PcG complexes have been shown to act as repressors of *Hox* gene expression (Fig. 1C; Akasaka et al. 1996). A significant, but substoichiometric amount, of Sf3b1 was reproducibly coimmunoprecipitated with Zfp144 and Rnf2, as revealed by comparison with anti-Rnf2 immunoblotting. The presence of ethidium bromide did not affect these Sf3b1–Zfp144/Rnf2 interactions, which suggests that they were DNA independent. As Sf3b1 is known to be a component of U2 snRNP (Krämer 1996; Schmidt-Zachmann et al. 1998), we therefore examined other U2 snRNP components, Sf3b4 (SAP49), U2B", and U snRNAs. In the conventional nuclear extracts, Sf3b4 was also coprecipitated with PcG proteins while anti-2,2,7-trimethylguanosine (TMG) antibody, which reacts to the 5' cap of U snRNAs characteristic for the U1, U2, U5, and U4/U6 snRNPs (Krämer 1996), failed to coprecipitate Rnf2. It is, however, possible that excess nucleoplasmic spliceosomal proteins or nucleoplasmic interaction between monomeric Sf3b1 and the PcG proteins would obscure experimental outcomes. To exclude these possibilities, we employed nuclear insoluble fraction extracted under high salt condition, in which proteins closely associated to chromatin are presumed to be concentrated. The fractions were solubilized by sonication and used in immunoprecipitation. Coimmunoprecipitation of Rnf2 with Phc1/Rae28 and Zfp144 indicated the presence of PcG multimeric complexes in this fraction. Sf3b1 and U2B" were coimmunoprecipitated with Phc1, Rnf2, and Zfp144. Concordantly, two different anti-Sf3b1 antibodies were able to coimmunoprecipitate Rnf2, reinforcing the interaction between Sf3b1 and PcG proteins. Notably, significant amounts of Rnf2 as well as Sf3b1 and U2B" were coimmunoprecipitated by anti-TMG antibody, implying the association of the U2 snRNA to PcG complexes. Importantly, these U2 snRNP components bound to the PcG proteins were detected in similar proportions (Fig. 1C,D). Taken together, these results show that it is likely that PcG complexes associate with at least part of the U2 snRNP rather than Sf3b1 alone.

To examine the biological implications of *Sf3b1*, we have generated an *Sf3b1*-mutant allele by replacing four exons with the *neo* gene in the opposite direction. *Sf3b1* null homozygotes died during preimplantation development around the 16- to 32-cell stage. Heterozygotes were externally normal and healthy, although the levels of *Sf3b1* mRNA and Sf3b1 were significantly reduced (Supplementary Fig. S1). Since *PcG* mutants exhibit posterior transformations of the vertebrae (Akasaka et al. 1996; Gould 1997; Suzuki et al. 2002), we examined axial skeletal preparations of $Sf3b1^{+/-}$ newborn pups backcrossed five times (N5) to C57BL/6 background. Significantly, $Sf3b1^{+/-}$ mice exhibited various skeletal alterations along the anterior–posterior axis (Table 1). In the cervical region of $Sf3b1^{+/-}$ mutants, the seventh cervical vertebra (C7) had incomplete ectopic ribs, either unilaterally or bilaterally fused with the first thoracic rib (27%), indicating transformations of C7 toward the first thoracic vertebra (T1) (Fig. 2B). Twenty-nine percent of $Sf3b1^{+/-}$ mutants had a prominent spinous process, characteristic for the second thoracic vertebra (T2), incorrectly associated with T1 (Fig. 2C), suggesting a T1 → T2

Table 1. *Summary of skeletal transformations in mutant mice*

Parents	B6 × *Sf3b1*$^{+/-}$ (N4)		*Mel18*$^{+/-}$ × *Sf3b1*$^{+/-}$ (N4)				*Mll*$^{+/-}$ × *Sf3b1*$^{+/-}$ (N6)			
Transformation types	wt (n = 50)	*Sf3b1*$^{+/-}$ (n = 48)	wt (n = 21)	*Mel18*$^{+/-}$ (n = 18)	*Sf3b1*$^{+/-}$ (n = 22)	*Mel18*$^{+/-}$*Sf3b1*$^{+/-}$ (n = 20)	wt (n = 14)	*Mll*$^{+/-}$ (n = 23)	*Sf3b1*$^{+/-}$ (n = 25)	*Mll*$^{+/-}$*Sf3b1*$^{+/-}$ (n = 15)
C7 → T1	0 (0)	27 (13)	0 (0)	6 (1)	32 (7)	45 (9), [a]4/9	0 (0)	0 (0)	68 (17)	0 (0)
T1 → T2	0 (0)	29 (14)	0 (0)	11 (2)	23 (5)	75 (15)	7 (1)	0 (0)	60 (15)	0 (0)
T13 → L1	0 (0)	6 (3)	0 (0)	28 (5)	14 (3)	50 (10)	0 (0)	9 (2)	8 (2)	13 (2)
L6 → S1	22 (11)	88 (42)	62 (13)	89 (16)	100 (22)	100 (20)	21 (3)	61 (14)	88 (22)	87 (13)

[a]Four out of nine C7 → T1 mice exhibited complete first ribs associated with the C7 vertebra (see Fig. 2G).
Unit: % (n).

transformation. In addition, *Sf3b1*$^{+/-}$ mice had only 12 ribs (6%) (Fig. 2F) and five lumbar vertebrae (88%) (Fig. 2E–F), indicating T13 → L1 and L6 → S1 transformations, respectively. Thus, *Sf3b1*$^{+/-}$ mice exhibit skeletal phenotypes similar to *PcG* mutants although the penetrance is rather low. We investigated next whether these skeletal alterations, seen with *Sf3b1*$^{+/-}$, were associated with anterior shifts of *Hox* gene expression boundaries as well as *PcG* mutants (Akasaka et al. 1996). The *Hoxb8* expression was extended to the seventh prevertebrae in three out of five *Sf3b1*$^{+/-}$ embryos and from the eighth prevertebra in wild type (Fig. 2L–N), and also *Hoxb6* and *Hoxc6* were ectopically expressed in the sixth prevertebrae in *Sf3b1*$^{+/-}$ embryos (Fig. 2I–K,O–Q). Significant changes were not observed for *Hoxa5*, *Hoxb3*, *Hoxb4*, or *Hoxd4* expression in the paraxial me-

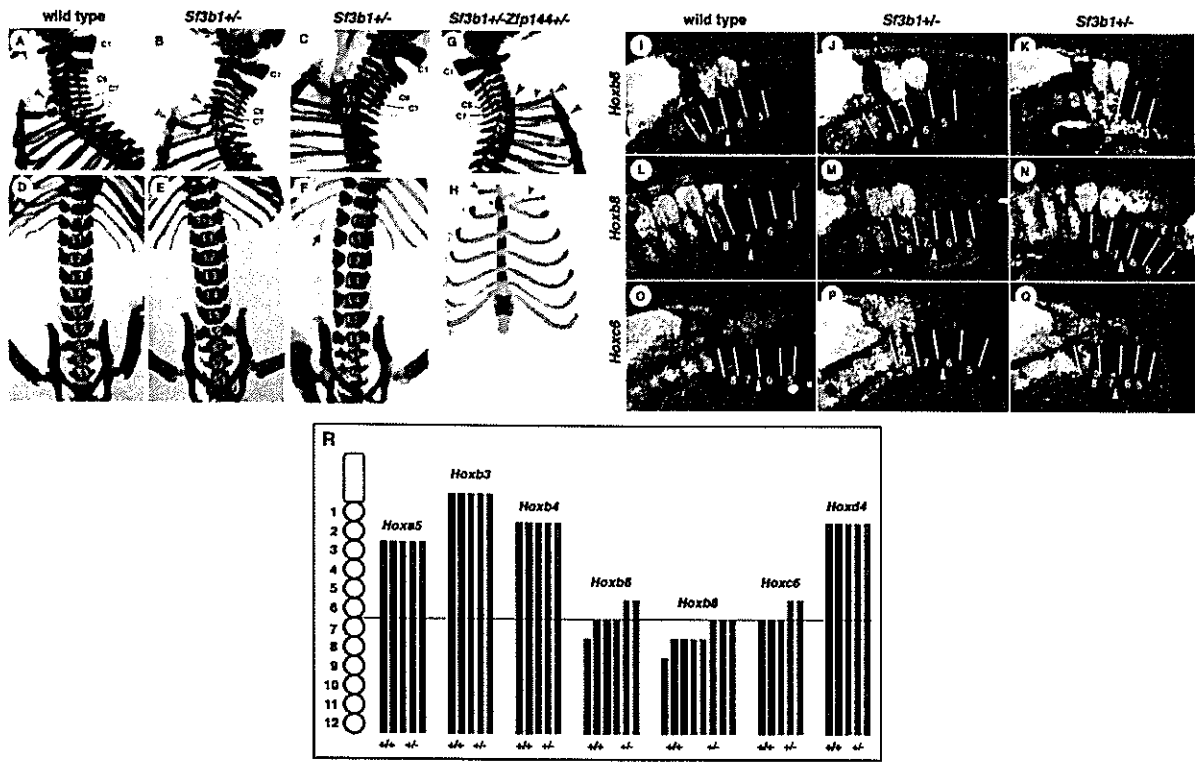

Figure 2. Skeletal abnormalities and ectopic *Hox* expressions in *Sf3b1*$^{+/-}$ mice. Cervical–thoracic (lateral view) and thoracic–sacral (ventral view) regions of wild-type (*A*,*D*) and two independent *Sf3b1*$^{+/-}$ (*B*,*C*,*E*,*F*) newborns are shown. Numbering of vertebrae of mutants makes them consistent with those of wild type. In wild type, C6 and T2 vertebrae have characteristic ventral processes as indicated by arrowheads (orange) and a prominent spinous process (yellow circle), respectively. An arrow indicates the disappearance of the T13 rib in the *Sf3b1*$^{+/-}$ mutant. (*G*,*H*) the lateral view of cervical–thoracic region and the ventral view of rib cage of the *Sf3b1*$^{+/-}$*Zfp144*$^{+/-}$ compound mutant. Ectopic ribs with C7 are represented by black arrowheads. An asterisk indicates an additional ossification center. Ribs numbered as 1–6 associate with T1–T6 vertebrae, respectively. The right ectopic rib with C7 separates from the rib with T1 on the sternum, as shown by green arrowheads. (*I*–*Q*) RNA in situ hybridization of *Hox* genes in embryos at 11.5 dpc. Boundaries of prevertebrae in lateral view are indicated by lines and the prevertebrae are numbered from prospective C1. Vertebral arteries are indicated by arrowheads and anterior boundaries of expressions are indicated by arrows. In *Sf3b1*$^{+/-}$ embryos, anterior boundaries of *Hoxb6*, *Hoxb8*, and *Hoxc6* expressions are shown to shift by sixth, seventh, and sixth prevertebrae, respectively. (*R*) Summary of *Hoxa5*, *Hoxb3*, *Hoxb4*, *Hoxb6*, *Hoxb8*, *Hoxc6*, and *Hoxd4* expressions in the paraxial mesoderm is depicted schematically. Each black (wild type) or gray (*Sf3b1*$^{+/-}$) bar represents expressional regions and a number of bars show individual embryos. Segment numbers are counted from the prospective C1.

soderm of *Sf3b1*$^{+/-}$ embryos (Fig. 2R). However, we found a subtle alteration of the *Hoxd4* expression in the second branchial arch of *Sf3b1*$^{+/-}$ embryos (data not shown). In summary, the expressions of several *Hox* genes were anteriorly extended in the paraxial mesoderm and second branchial arch in *Sf3b1*$^{+/-}$ embryos. These observations are consistent with the axial skeletal alterations observed in *Sf3b1*$^{+/-}$ mice. Therefore, we concluded that Sf3b1 mediates the repression of *Hox* genes.

Individual *PcG* mutations have been shown to mutually enhance their phenotypes (Bel et al. 1998; Akasaka et al. 2001; Suzuki et al. 2002). To investigate whether this Sf3b1-mediated repression involves PcG complexes, we examined the genetic interactions between *Zfp144* and *Sf3b1* mutations. In *Sf3b1*$^{+/-}$*Zfp144*$^{+/-}$ double heterozygotes, the formation of an additional ossification center in the sternum, and the detachment of the ribs of T7 from the sternum, represented an anterior shift of the sternum of one segment width (Fig. 2H). The ectopic ribs associated with C7 mimicked perfect ribs and formed joints with the anteriorly shifted sternum (Fig. 2G). These alterations were observed in four (44%) out of nine double mutants that displayed perfect C7 → T1 transformation but were not observed in either of the single mutants (Table 1). In addition to the ectopic ribs, the frequencies of other transformations were much higher in the double mutants. In particular, the T1 → T2 transformation occurred at a much higher penetrance: 75% in double mutants versus only 11% or 23% in either single mutant, suggesting that the single phenotypes of respective mutations were enhanced in the presence of each other. We further examined the impact of the *Sf3b1* mutation on the mutation at the *mixed lineage leukemia* (*Mll*) gene (Yu et al. 1995), a mammalian homolog of the *trithorax* gene of *Drosophila melanogaster*, whose product is antagonistic to *PcG* mutations (Hanson et al. 1999). Posterior transformations at the cervico–thoracic transitional zone caused by *Sf3b1* mutation were completely restored by *Mll* mutation (Table 1; Yagi et al. 1998). Therefore, it is likely that Sf3b1 has an antagonistic relationship to trxG proteins as well as PcG complexes. Taken together, these results indicate that Sf3b1 is functionally involved in PcG repressive complexes.

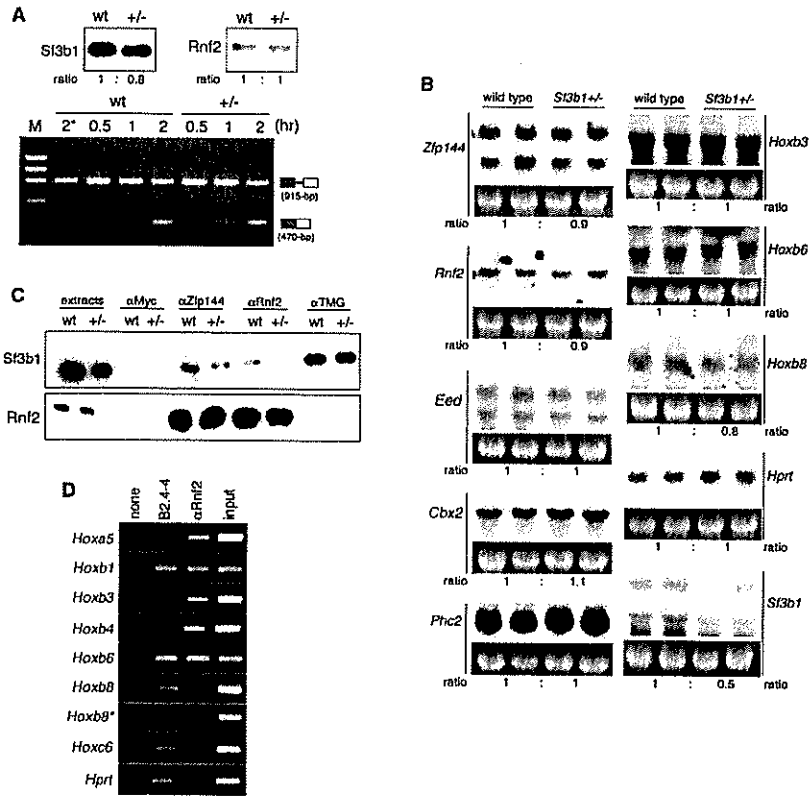

Figure 3. Comparison of wild-type and *Sf3b1*$^{+/-}$ embryos. Genotyping of embryos was performed with total DNA from yolk sacs. (*A*) In vitro splicing assay. The soluble fraction of a nuclear extract was prepared from wild-type or *Sf3b1*$^{+/-}$ embryos at 10.5 dpc. Equal amounts (60 μg) of total protein were confirmed by Western blotting with anti-Sf3b1 and anti-Rnf2 antibodies (*upper* panels) and subjected to a splicing assay (*lower* panel). One-step RT–PCR revealed that unspliced forms consisting of two exons and an intron (upper bands) as the RNA substrates were converted into spliced forms (lower bands) by the splicing reaction. Band intensities were measured by the image-processing program Image J and the ratios of *Sf3b1*$^{+/-}$ to wild type were obtained.(*B*) Northern analysis of total RNAs (15 μg each) from independent embryos at 12.5 dpc. Ethidium-bromide-stained 28S rRNAs prior to transfer to membranes are displayed *below* their blots. Intensity of each detected band was normalized by their rRNAs and then the ratios of *Sf3b1*$^{+/-}$ to wild type were calculated (indicated *below* their panels). (*C*) Immunoprecipitation assay with embryos at 11.5 dpc. Three independent embryos with the same genotype were sonicated individually, and the soluble lysates were mixed and then divided into four. Each was immunoprecipitated with a specific antibody. (*D*) ChIP assay with ES cells. Cross-linked chromatins were immunoprecipitated with or without indicated antibodies and subjected to amplification of *Hox* and *Hprt* regions (260–480 bp) by PCR. The amplified regions were detected in 1.5% agarose gels.

Since Sf3b1 is involved essentially in pre-mRNA splicing, the basal expression levels of genes, including *PcG* or *Hox* genes, may be profoundly altered in *Sf3b1*$^{+/-}$ mice, leading to homeotic transformations. To investigate this, a basal activity of splicing was examined with nuclear extracts from 10.5 dpc *Sf3b1*$^{+/-}$ embryos in which the Sf3b1 level was reduced up to ~75% but Rnf2 accumulated at normal level (data not shown). Despite such lower quantities of Sf3b1, their splicing activity was equal because of the same ratio of their spliced forms (Fig. 3A). Furthermore, while expression levels of *Sf3b1* were reduced by half in *Sf3b1*$^{+/-}$ embryos, those of five PcG genes, *Zfp144*, *Rnf2*, *Eed*, *Cbx2/M33*, and *Phc2/Edr2*; three *Hox* genes, *Hoxb3*, *Hoxb6*, and *Hoxb8*; and a metabolic gene, *Hprt*, were not (Fig. 3B). Thus, homeotic transformations in *Sf3b1*$^{+/-}$ mice appear to be independent of the alteration of general gene expression. Next, we investigated the amount of Sf3b1 associated with PcG proteins in *Sf3b1*$^{+/-}$ embryos. While Zfp144- or Rnf2-associated Sf3b1 were clearly decreased in *Sf3b1*$^{+/-}$ embryos, Rnf2 was precipitated equally in both embryos (Fig. 3C). It was also notable